nature ecology & evolution

Article

https://doi.org/10.1038/s41559-022-01893-x

Abiotic conditions shape spatial and temporal morphological variation in North American birds

Received: 15 March 2022

Accepted: 30 August 2022

Published online: 27 October 2022

Check for updates

Casey Youngflesh $\mathbb{O}^1 \boxtimes$, James F. Saracco \mathbb{O}^2 , Rodney B. Siegel² and Morgan W. Tingley \mathbb{O}^1

Quantifying environment-morphology relationships is important not only for understanding the fundamental processes driving phenotypic diversity within and among species but also for predicting how species will respond to ongoing global change. Despite a clear set of expectations motivated by ecological theory, broad evidence in support of generalizable effects of abiotic conditions on spatial and temporal intraspecific morphological variation has been limited. Using standardized data from >250,000 captures of 105 landbird species, we assessed intraspecific shifts in the morphology of adult male birds since 1989 while simultaneously measuring spatial morphological gradients across the North American continent. We found strong spatial and temporal trends in average body size, with warmer temperatures associated with smaller body sizes both at more equatorial latitudes and in more recent years. The magnitude of these thermal effects varied both across and within species, with results suggesting it is the warmest, rather than the coldest, temperatures that drive both spatial and temporal trends. Stronger responses to spatial-rather than temporalvariation in temperature suggest that morphological change may not be keeping up with the pace of climate change. Additionally, as elevation increases, we found that body size declines as relative wing length increases, probably due to the benefits that longer wings confer for flight in thin air environments. Our results provide support for both existing and new large-scale ecomorphological 'rules' and highlight how the response of functional trade-offs to abiotic variation drives morphological change.

Morphology is both a cause¹ and a consequence² of how organisms interact with their environment. Assessing patterns in morphological variation both across and within³ species provides a means to better understand these interactions and, consequently, predict ecological responses to environmental change. Ecological theory suggests that both the sizes and shapes of organisms should vary across latitude (for example, Bergmann's⁴ and Allen's⁵ rules) and also possibly elevation,

particularly for flying organisms (due to lower temperatures and lower air density at high elevations 6). These ecogeographic expectations are commonly used to motivate hypotheses for how species will respond to climate change 7 , such as the suggestion that declining body size may be a generalized response of endotherms to warming temperatures 8 . However, an holistic understanding of generalizable spatiotemporal effects of abiotic conditions on intraspecific morphological variation

¹Department of Ecology and Evolutionary Biology, University of California, Los Angeles, Los Angeles, CA, USA. ²The Institute for Bird Populations, Petaluma, CA, USA. —e-mail: caseyyoungflesh@gmail.com

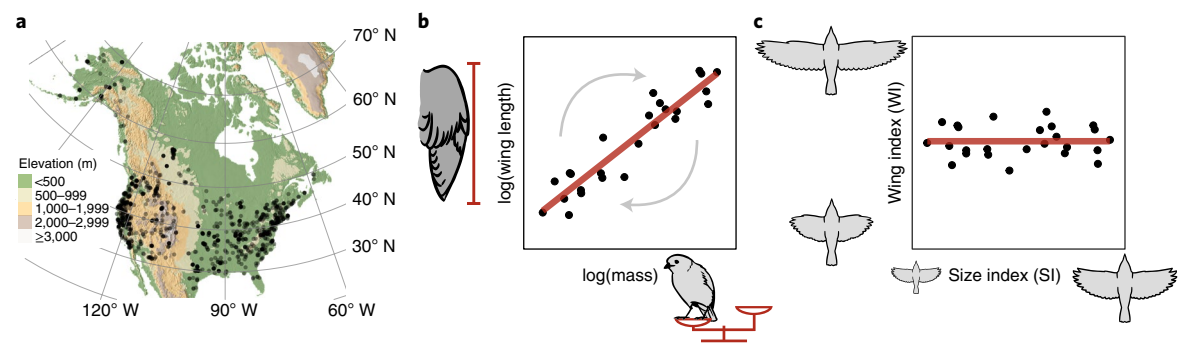


Fig. 1| The MAPS dataset provides a large spatial-, temporal- and taxonomic scale resource for studying avian morphological variation over time and space. a, Data on individual birds come from 1,124 MAPS banding stations (black points) spanning the latitudinal and elevational extent of North America. **b**, Measurements were taken for both wing length (chord of the unflattened wing) and mass for each captured bird. On the basis of allometric scaling principals and empirical measurements across species, wing length is expected to be proportional to mass to the one-third power (the scaling exponent in the

power law equation); logging both variables linearizes this relationship. Points represent individuals from a single hypothetical species. **c**, The scaling exponent was used to create a rotation matrix which was applied to logged wing length and logged mass for each species, to derive two independent morphological indices: size index (SI) and wing index (WI), denoting the overall size of each individual bird and the degree to which wing length deviates from its expected value given the body mass of the individual, respectively. For additional details on this mathematical transformation, see Extended Data Fig. 2.

has been limited by a lack of taxonomic and spatial replication, with studies yielding conflicting results $^{8-11}$. Understanding the role that abiotic factors play in shaping morphological traits, as well as how and why this varies over space and time, is of particular importance for North American birds, which have precipitously declined in abundance over a period coincident with modern anthropogenic warming 12 .

We evaluated spatiotemporal morphological variation in 105 North American bird species over 30 years (1989–2018), across more than 43° of latitude and nearly 3,000 m of elevation, using data from more than 250,000 live birds, primarily passerines or near-passerines, captured during the breeding season using standardized methods13 (Fig. 1a, Extended Data Fig. 1 and Supplementary Table 1). Using field measures of body mass and wing length (length of the unflattened, closed wing) in conjunction with allometric scaling theory¹⁴, we derived two morphological indices, a size index (SI) and a wing index (WI) (Fig. 1b,c). SI and WI reflect overall bird body size and 'wingyness' (wing length relative to body mass), respectively (Extended Data Fig. 2) and were used to account for the fact that mass and wing length are intrinsically linked (that changes in mass may be due to changes in wing length and vice versa). Using a hierarchical Bayesian approach to estimate species-specific responses, we modelled these indices as a function of year, latitude and elevation and estimated and compared the impact of spatial and temporal variation in temperature on adult male bird body size.

Results and discussion

Morphological variation over time

On average, across the wide spatial and taxonomic breadth of sampling, avian body size decreased over time (SI μ_{RIDX} (equation (10)) = -0.03 SI per 10 years, 89% confidence interval (CI) (-0.04, -0.01), $P(\mu_{\eta_{\text{IDX}}} < 0) = 1$; Fig. 2a and Supplementary Table 2). Some variation in this trend existed across species, with decreases observed for 80 of the 105 focal species (Supplementary Table 2 and Extended Data Fig. 3a). Absolute body mass showed range-wide declines of up to 2.78% between 1989 and 2018 (for example, tree swallow *Tachycineta bicolor*, ω_{MTIME} (equation (25)) = -2.78, 89% CI (-4.98, -0.63), $P(\omega_{\text{MTIME}} < 0) = 0.98$), with a mean decline in mass of 0.56% across all species ($\mu_{\omega_{\text{MTIME}}}$ (equation (26)) = -0.56, 89% CI (-0.78, -0.34), $P(\mu_{\omega_{\text{MTIME}}} < 0) = 1$; Extended Data Fig. 7a, Supplementary Table 3). This temporal trend toward smaller bodies for most species and over most of a continent is likely the result of warming temperatures. Specifically, smaller body sizes were associated with elevated temperatures in the year of capture ($\mu_{\gamma_{\text{TYT}}}$ lag 0 (equation (15)) = -0.019 SI per 1 °C, 89% CI

 $\begin{array}{l} (-0.022,-0.016), P(\mu_{\gamma_{\text{TVT}}} \log 0 < 0) = 1), \text{as well as 1 year before capture} \\ (\mu_{\gamma_{\text{TVT}}} \log 1 = -0.007, 89\% \text{ CI } (-0.010,-0.004), P(\mu_{\gamma_{\text{TVT}}} \log 1 < 0) = 1); \end{array}$ posterior mean estimates for the species-specific effect of temperature on body size (γ_{TVT} (equation (15))) were negative for 100% of species for temperature in the year of capture and for 92% of species for temperature in the year before capture (Supplementary Table 4 and Extended Data Fig. 5a). Temperatures 2 years before capture were not strongly related to body size ($\mu_{\gamma_{TVT}}$ lag 2 = 0.001, 89% CI (-0.002, 0.004), $P(\mu_{\gamma_{\text{TVT}}} \log 2 < 0) = 0.26$; Fig. 2b, Extended Data Fig. 5 and Supplementary Table 4). Temperatures 1 and 2 years before capture correspond to environmental conditions likely experienced during ontogenesis, although postnatal dispersal limits the strength of this inference from banding data. Nevertheless, our findings align with expectations, given that smaller-bodied individuals-having larger surface-area-to-volume ratios-tend to have lower cooling costs compared to larger-bodied individuals. This also agrees with previous work that observed changes in both bird mass^{11,15} and surface area in response to rising temperatures 16 and provides strong support for the hypothesis that shrinking body size is a generalized response to climate change^{7,8}.

Temperature-mediated size-dependent mortality (which may result in directional selection, conditional on the heritability of body size: for example ref. ¹⁷) and/or developmental plasticity during early life stages¹⁸ may be the most likely proximate drivers of our finding of an association between warmer temperatures and smaller bodies. Although widespread evidence for adaptive evolutionary responses to climate change is somewhat limited 19,20, the rate of morphological change reported here is within the range that might be expected via evolutionary change (Extended Data Fig. 9). The lack of a strong relationship with temperatures 2 years before capture could suggest that a large portion of measured individuals were in their second year of life and never experienced the conditions 24 months before. Greater effects of temperature on body size in the warmer portions of species' ranges ($\mu_{\theta_{\text{TVT}}}$ lag 0 (equation (15)) = -0.012 unit change in effect of temperature per 10 °C change in mean site temperature, 89% CI (-0.023, -0.001), $P(\mu_{\theta_{TVT}} \log 0 < 0) = 0.96$; Fig. 2c) suggests that it is the hottest experienced temperatures-rather than the coldest-that are driving this body size-temperature association²¹. This effect was less pronounced for temperatures in the year before and 2 years before capture ($\mu_{\theta_{\text{TVT}}}$ lag 1 = -0.010, (89% CI -0.021, 0.001), $P(\mu_{\theta_{\text{TVT}}} \log 1 < 0) = 0.93; \mu_{\theta_{\text{TVT}}} \log 2 = -0.004, 89\% \text{ CI } (-0.014, 0.006),$ $P(\mu_{\theta_{\text{TVT}}} | \text{lag } 2 < 0) = 0.75$; Fig. 2c). Although poleward range shifts of species could also result in directional change in morphology at a given location, declines in body size in even the warmest portions of species'

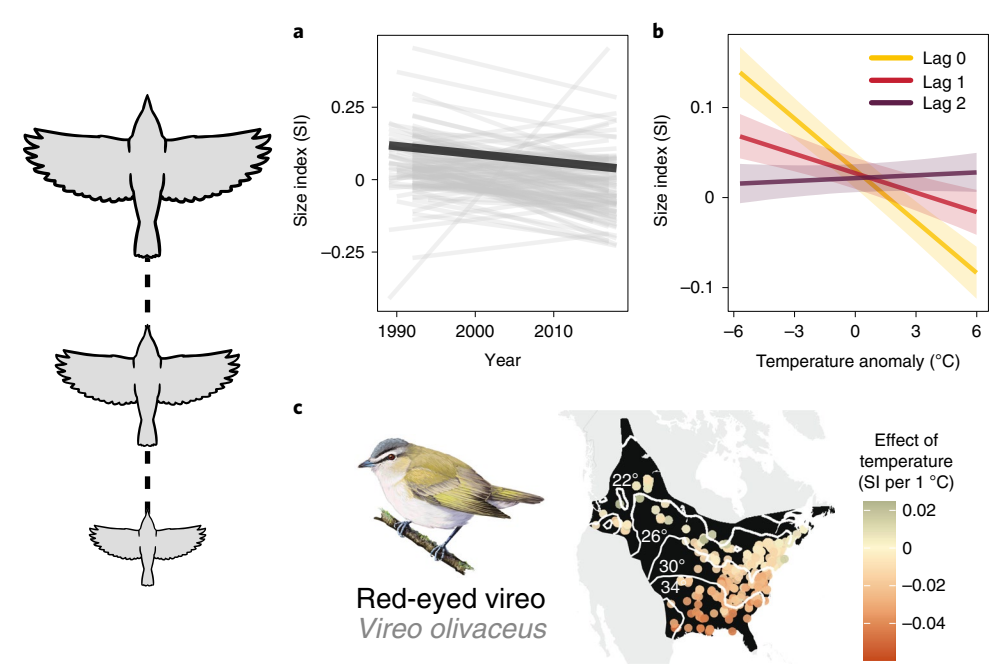


Fig. 2 | North American birds show an average decline in body size (SI) over time and in response to temporal fluctuations in temperature. a, Change in SI over time for 105 species, controlling for changes over latitude and elevation. Each thin grey line represents the trend for one species and the thick black line represents the mean trend across all species. b, Change in SI across species in response to interannual fluctuations in May–July maximum temperature in the year of capture ($lag\ 0$) as well as $1\ year\ (lag\ 1)$ and $2\ years\ (lag\ 2)$ before capture.

Ribbons represent 89% Cls. \mathbf{c} , Effect of 1 °C change in temperature on SI at capture locations for a representative species, the red-eyed vireo *Vireo olivaceus*, showing stronger effects of temperature on SI in warmer areas. Darker, orange hues represent a stronger negative effect of temperature on SI. The black polygon represents the range of the species and white lines (and associated white text) represent isoclines for May–July maximum temperature in a single year, 2018.

ranges (where individuals are generally smallest) suggests that dispersal is not the primary mechanism driving these observed changes.

In contrast to shrinking body size in North American birds, we found that the wingyness (wing length relative to body mass) of birds has increased over time (WI $\mu_{\eta_{\rm IDX}}$ (equation (10)) = 0.02 WI per 10 years, 89% CI (0.00, 0.03), $P(\mu_{\eta_{\text{IDX}}} > 0) = 0.95$; Extended Data Fig. 4a and Supplementary Table 2). Although this pattern could be due to changing migratory patterns in response to ongoing range shifts²², constraints on the rate at which wing length can change over time compared to body size^{23,24} might also play a role. Specifically. we observed no change in absolute wing length over time-temporal changes in wingyness were the result of declining mass ($\mu_{\omega_{\rm M_{TIME}}}$ (equation (26)) = -0.56% change over study period, 89% CI (-0.78, -0.34), $P(\mu_{\omega_{\text{TIME}}} < 0) = 1)$ with relatively stable wing length $(\mu_{\omega_{\text{WIJME}}}$ (equation (26)) = -0.01% change over study period, 89% CI (-0.13, 0.12), $P(\mu_{\omega_{\text{WIJME}}})$ = 0.54; Extended Data Figs. 7a and 8a and 8. Supplements of Taking 2. Supplementary Table 3). That is, while birds have, on average, become smaller, their wings have stayed relatively the same size, in agreement with research from the Middle East 16. Other North and South American studies, however, have observed increases in wing length over time^{11,15}. In the case of ref. 11-the closest comparison to this study—the discrepancy in findings may be due to the limitations of sampling at a single location during the breeding season, which might result in sampling different populations over time. However, these differences might also reflect the complexities of morphological variation and how these patterns might vary over time and space. For example, the rate at which morphology changes might vary over space (i.e., exhibit spatial non-stationarity²⁵), leading similar studies to come to different conclusions on the basis of their study area of interest.

Morphological variation over latitude

Why is it so critical to control for geography when assessing temporal trends in phenotypes? Bird morphology shows strong and

generalizable trends in morphology over space. As illustrated by our dataset across 105 bird species and most of a continent, body size strongly increases with latitude (SI $\mu_{\gamma_{\rm IDX}}$ (equation (11)) = 0.37 SI per 10° of latitude, 89% CI (0.29, 0.45), $P(\mu_{\gamma_{\rm IDX}} > 0) = 1$; Fig. 3a, Extended Data Fig. 3b and Supplementary Table 2), supporting the intraspecific interpretation of Bergmann's rule⁴, despite decades of debate on its relevance 26 . On average, body mass increases 5.72% ($\mu_{\omega_{\rm M_{IAT}}}$ (equation (26)) = 5.72%, 89% CI (5.39, 6.04), $P(\mu_{\omega_{M_{1AT}}} > 0) = 1$; Extended Data Fig. 7b and Supplementary Table 3) over the sampled latitudinal range of a given species. Larger body sizes are associated with regions with cooler average temperatures (SI $\mu_{\beta_{SVT}}$ (equation (20)) = -0.37 SI per 10 °C of change in mean site temperature, 89% CI (-0.46, -0.29), $P(\mu_{\beta_{\text{SVT}}} < 0) = 1$; Fig. 3b and Extended Data Fig. 6) that are generally found at higher latitudes, supporting the notion that thermal factors play a substantial role in governing body size not only over time but also over space²¹. Additionally, we found that this relationship between temperature and spatial variation in body size is stronger for species that experience warmer conditions (θ_{SR} (equation (22)) = -0.29 unit change in effect of temperature per 10 °C of change in mean range-wide temperature, 89% CI (-0.49, -0.09), $P(\theta_{SR} < 0) = 0.99$; Fig. 3b), illustrating—as with findings of temporal associations between body size and temperature—that the warmest, rather than the coldest, temperatures probably drive intraspecific adherence to Bergmann's rule.

Factors other than temperature may also be important in driving morphological variation. For example, some evidence exists for an increase in wingyness with latitude (WI μ_{PIDX} (equation (11)) = 0.04 WI per 10° of latitude, 89% CI (0.00, 0.07), $P(\mu_{\text{PIDX}}>0)=0.92$; Extended Data Fig. 4b and Supplementary Table 2). While thermal factors might suggest that appendages should be smaller towards the poles to limit heat loss—known as Allen's rule $^{5.27}$ —the length of the closed bird wing is primarily a function of flight feather length. This may obscure the relationship between appendage size and temperature in this case, a relationship that is well supported for bird bill size (an anatomical

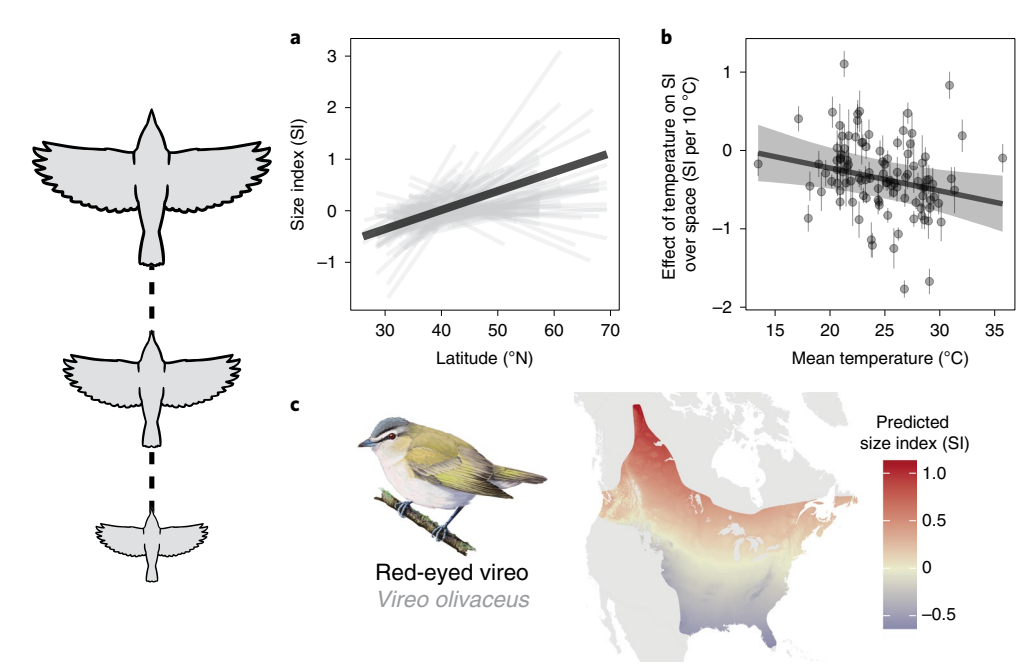


Fig. 3 | **On average, avian body size (SI) increases over latitude and with colder temperatures. a**, Change in SI over latitude for 105 species, controlling for changes over time and elevation. Each thin grey line represents the trend for one species and the thick black line represents the mean trend across all species. **b**, The effect of temperature on variation in SI across space within each species as a function of the mean (range-wide) temperature experienced by that species. Each point represents a single species. Grey vertical bars represent one posterior standard deviation of the effect of spatial variation in temperature

on SI, the thick black line represents the linear model fit and the grey ribbon represents the 89% CI. The body size–temperature relationship is stronger for species that experience warmer temperatures. **c**, Predicted body size (SI) over the range of a representative species, the red-eyed vireo *V. olivaceus*, based on the estimated effect of latitude and elevation. Yellow hues represent average, red hues represent larger than average and blue hues represent smaller than average predicted SI.

structure which readily dissipates heat)27. Relatively longer wings at higher latitudes may reflect the longer distances that breeding birds from more northerly populations tend to travel to complete their migration. Longer and more pointed wings are thought to increase the efficiency of long flights and are generally found in populations that migrate longer distances²⁸⁻³⁰. For some species, populations breeding at higher latitudes migrate farther than southern populations, yielding 'leapfrog' migration patterns; for other species, equatorward populations of an otherwise migratory species remain non-migratory³¹. Indeed, species known to exhibit leapfrog migrations (for example, Wilson's warbler Cardellina pusilla³² and fox sparrow Passerella ili aca^{33}), as well as migratory species with resident populations in the southern portions of their ranges (for example, Eastern towhee Pipilo erythrophthalmus³⁴ and white-eyed vireo Vireo griseus³⁴), here show pronounced increases in wingyness with latitude (Extended Data Fig. 4b and Supplementary Table 2). Smaller or even negative effects of latitude for other species might be indicative of alternative migration strategies-in which northerly populations do not migrate longer distances than southerly populations³¹—as well as the importance of other factors, such as variation in habitat structure³⁵ and/or predation³⁶, that might also drive variation in wing length.

Morphological variation over elevation

Less well understood is how morphology varies over elevation. Given decreasing temperatures at high elevations, body size might be expected to increase (Bergmann's rule applied to elevation). However, we find that body size generally decreases with elevation (SI $\mu_{\theta_{\text{IDX}}}$ (equation (11)) = -0.06 SI per 1,000 m, 89% CI (-0.12, 0.00), $P(\mu_{\theta_{\text{IDX}}} < 0) = 0.96$; Extended Data Fig. 3c and Supplementary Table 2), indicating that, contrary to the general associations found between body size and temperature over space, pressures unrelated to thermoregulation dominate over this gradient (potentially reflecting

lower resource availability at higher elevations³⁷). Species with wide elevational gradients may therefore rely on a variety of behavioural adaptations, such as facultative altitudinal migration^{38,39} and even nightly torpor⁴⁰, to cope with lower temperatures at higher elevations.

In contrast to body size, wingyness strongly increases with elevation (WI $\mu_{\theta_{\text{IDX}}}$ (equation (11)) = 0.32 WI per 1,000 m, 89% CI (0.28, 0.37), $P(\mu_{\theta_{\text{IDX}}} > 0) = 1$; Fig. 4, Extended Data Fig. 4c and Supplementary Table 2). Elevational trends in both indices are due to countervailing changes in absolute morphology: body mass decreases ($\mu_{\omega_{\text{MELEV}}}$ (equation (26)) = -1.15% change over species' elevational range, 89% CI (-1.42, -0.89), $P(\mu_{\omega_{\text{MELEY}}} < 0) = 1$; Extended Data Fig. 7c and Supplementary Table 3) while wing length increases with elevation ($\mu_{\omega_{\text{WELEV}}}$ (equation (26)) = 2.15% change, 89% CI (2.00, 2.30), $P(\mu_{\omega_{\text{WELEV}}} > 0) = 1$; Extended Data Fig. 8c and Supplementary Table 3). These elevational ecogeographic relationships for birds are likely due to the key role that air pressure plays in flight performance. Air density, a key determinant in the amount of lift that a wing produces, is lower at higher elevations, necessitating some compensatory measures to maintain flight (i.e., more relative power output via larger wings and/or lower mass, larger wing stroke amplitude or increased wingbeat frequency^{6,41}).

While large-scale increases in wing size with elevation have been documented previously, this pattern was (incorrectly) taken to be indicative of an increase in the size of individuals⁴². Our results illustrate a clear increase in wing length with elevation independent of any changes in body size (Fig. 4), providing large-scale, cross-taxonomic evidence for this heretofore unrecognized ecomorphological gradient. This intraspecific pattern of increased wing length with elevation harmonizes observations in some insects⁴³, among specific groups of bird species, including hummingbirds (family Trochilidae⁴⁴) and white-eyes (*Zosterops* spp. ⁴¹) and from a limited number of single-species studies (for example, song sparrow *Melospiza melodia*⁴⁵ and Eurasian tree sparrow *Passer montanus*⁴⁶).

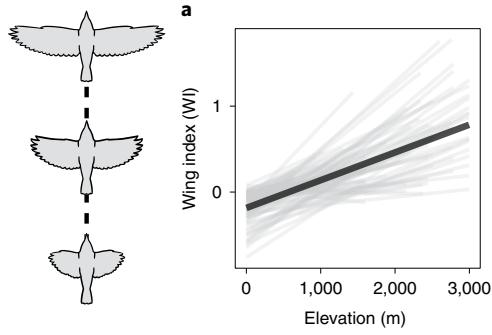




Fig. 4 | **Avian wing index (WI) increases with elevation, showing strong continental spatial patterns. a**, Change in WI over elevation for 105 species, controlling for changes over time and latitude. Each thin grey line represents the trend for one species and the thick black line represents the mean trend across all

species. **b**, Predicted wingyness (WI) over the range of a representative species, the northern parula *Setophaga americana*, based on the estimated effect of latitude and elevation. Yellow hues represent average, red hues represent larger than average and blue hues represent smaller than average predicted WI.

Implications for understanding the impacts of global change

While intraspecific morphological differences are often disregarded in macroecological and functional studies, this important element of biodiversity has major implications for understanding how organisms are shaped by their environments, how they are likely to respond to future global change and for the conservation of natural systems⁴⁷. For example, the degree to which species can respond to the thermoregulatory pressures caused by warming temperatures may impact their ability to persist in their current ranges²¹. More frequent extreme weather events that may result in large-scale thermoregulatory-related mortality events⁴⁸ and chronic sublethal effects of increased temperature may have pronounced effects on populations⁴⁹. While body size in North American birds has responded to warming temperatures over time, larger responses to temperature variation over space compared to temperature variation over time suggest that the rate of morphological change over time may be evolutionarily and/or plastically constrained. Specifically, the average SI response to spatial variation in temperature was almost twice as large as the average SI response to temporal variation in temperature in the year of capture (spatial: $\mu_{\beta_{ ext{SVT}}}$ (equation (20)) = -0.37; temporal: $\mu_{\gamma_{\text{TVT}}}$ (equation (15)) = -0.19; Fig. 5a)—this effect would be even more pronounced for temperature in the year before capture. Overall, 69% of species responded more strongly to temperature variation over space compared to variation over time (Fig. 5b). This raises concern that species may not be responding rapidly enough over time to keep pace with ongoing climatic change⁵⁰ The potential for mismatch between species and their environments is especially concerning for some bird species-including those living in hot, arid environments, such as lesser goldfinch (Spinus psaltria) and chipping sparrow (Spizella passerina)—that may lack suitable microrefugia in portions of their ranges to buffer them from especially warm temperatures⁵¹.

Conclusions

Morphological responses to thermoregulatory pressures, as well as the importance of flight efficiency, illustrate how interacting functional trade-offs contribute to observed morphological variation (Extended Data Fig. 10). Other factors not directly considered in this study, including additional thermoregulatory factors (for example, minimum rather than maximum temperatures), habitat characteristics and conditions experienced on overwintering grounds, likely act in concert with these processes to shape variation within and among species. Characterizing the interplay between these various factors, operating over space and time, is key to understanding how morphology is likely to change into the future, in response to continued abiotic environmental change. Although the ecological consequences of morphological change and how morphology interacts with other climate change responses—including shifts in species' ranges ⁵² and the timing

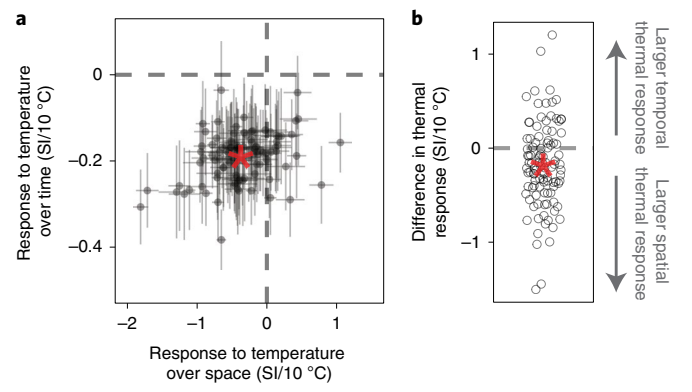


Fig. 5 | Avian body size (SI) shows a stronger response to spatial, compared to temporal, variation in temperature, indicating a failure of species to track temperature increases as much as expected. a, Change in SI per 10 °C change over time (at lag 0; γ_{TVT} (equation (15))) plotted against change in SI per 10 °C change over space (β_{SVT} (equation (19))). Dots represent posterior means for each species and error bars represent one posterior standard deviation. The red star represents the cross-species mean. b, The difference between the response to spatial variation in temperature and the response to temporal variation in temperature. Negative values represent larger (more negative) responses of SI to spatial variation in temperature, while positive values represent larger responses of SI to temporal variation temperature. Open circles represent the posterior mean for each species, while the red star represents the cross-species mean difference.

of seasonal events⁵³—are currently unknown⁸, the importance of body size for life history traits⁵⁴, physiology⁵⁵ and both cross-trophic⁵⁶ and intra-trophic⁵⁷ interactions, suggests that the implications of these changes could be far reaching. Given projected changes in climatic conditions, continued morphological change and its associated consequences can be expected.

Methods

Morphological data

Bird morphology data were collected as part of the Monitoring Avian Productivity and Survivorship (MAPS) programme, a collaborative long-term bird-banding project operating across North America¹³. Data were obtained from 1,124 banding stations (Fig. 1), each consisting of 6–20 mist nets, over the period 1989–2018 (although most stations operated during only a subset of this period). Banding stations were operated 6–12 times per year, from 1 May to 28 August¹³, encompassing the breeding season for most birds in North America. Only records obtained within species' breeding ranges were used (as determined annually by banding station operators). While our dataset does not span

the entire breeding range of every species, this lack of complete coverage is unlikely to bias results given the flexible analytical framework we use, which allows us to account for spatiotemporal heterogeneity in these data. Limited sampling at very high latitudes, however, prevents us from making inference in these areas. For each captured bird, wing length (distance between the carpal joint and the wing tip, commonly referred to as unflattened wing chord) was measured to the nearest millimetre following ref. ⁵⁸ and body mass was recorded to the nearest 0.5 g (ref. ¹³). Birds were aged following criteria summarized by ref. ⁵⁸.

We restricted our analyses to male birds classified as 'after hatch year' (captured at least one breeding season after the hatch year of the bird) to avoid any confounding morphological variation among age classes and between sexes and changes in female bird mass throughout the season that may be due to egg production and laying. Other factors, such as variation in food availability across the season, the energetic demands of nesting or moult status, might contribute to noise in these data, although should not bias measures in any way. All records with body mass or wing length measurements that were more than five median absolute deviations (MAD⁵⁹) away from the median were excluded, as these probably represented measurement or data entry errors. If an individual was captured more than once in a season, only measurements taken during the initial capture were considered. Only species for which data were available for at least 375 captures (after data filtering) were analysed. In total, morphological data from 253,488 captures of 105 species, representing two orders and 18 taxonomic families were used from banding stations spanning more than 43° of latitude (26.1° N to 69.4° N) and 2,996 m of elevation (Supplementary Table 1).

Elevation data

Elevation data for each banding station were obtained from the 30 arcsec resolution (-1 km at the equator) global multi-resolution terrain elevation data 2010 data product 60 .

Temperature data

Daily maximum temperature data for each banding station were obtained over the study period from the 1 km gridded Daymet surface weather data product⁶¹. For each year at each site, we calculated the average maximum temperature from ordinal day (day of year) 121 to ordinal day 212 (1 May to 31 July in a non-leap year). We refer to this annual metric as 'May-July maximum temperature'. We use this time window as it generally encompasses the incubation and nestling stages for these species³⁴, where birds are generally constrained to be at or near their nests. During this period, there may be fewer opportunities to take advantage of microrefugia that might buffer individuals from the effects of temperature. We calculated the mean May-July maximum temperature across years at each station as well as year-specific values for temperature at each station to evaluate the effect of temperature on morphological variation across space and time, respectively. Species-wide mean temperature values were calculated by taking the mean May-July maximum temperature across all stations for each species.

Derivation of morphological indices

Two morphological indices were derived from data collected on body mass and wing length for each bird. The size index (SI) corresponds to the overall size of an individual, while the wing index (WI) corresponds to the relative (to body mass) wing length, or 'wingyness', of each individual. These indices were derived using the expected power law 62,63 relationship between these two traits,

$$W = bM^c, (1)$$

where Wis wing length, Mis body mass, b is a scalar and c is the scaling exponent (Fig. 1b,c and Extended Data Fig. 2), denoting how rapidly

wing length increases as a function of mass. This relationship is linearized when taking the log of both sides of the equation,

$$\log(W) = \log(b) + c \times \log(M). \tag{2}$$

Using species-level mean values for both log(W) and log(M), we estimated the scaling exponent by applying a phylogenetic regression (to control for the effect of phylogenetic relatedness on parameter estimates⁶⁴) using the 'caper' package⁶⁵ in R (ref. ⁶⁶) to the linearized form of the power law relationship (equation (2)). Species-level mean values were used because we were interested in understanding the general relationship between wing length and body mass and in validating theoretical expectations of the relationship between these traits. This scaling exponent represents the null expectation for how wing length covaries with mass, whether that be within or across species. We use this null expectation to derive wing and size indices to then explore how the relationship between these traits varies within species across time and space. We estimated the scaling exponent for each of 100 phylogenetic trees for the species of interest obtained from Bird-Tree⁶⁷ (www.birdtree.org) to account for uncertainty in the phylogenetic relatedness of these species. The mean of the 100 estimates (mean = 0.333, s.d. = 0.002) of the empirical relationship between wing length and body mass (the scaling exponent) was nearly identical to the theoretical expectation, given isometric scaling principles (where $c = \frac{1}{2}$; mass is expected to be proportional to volume, which scales as the cube of a linear dimension, such as wing length) and similar to estimates from other studies^{68,69} (Extended Data Fig. 2).

For each species, measurements of body mass and wing length of individual bird captures were then reprojected onto new axes using a rotation matrix derived from the estimated scaling exponent (the rate at which wing length is expected to change with body mass). The rotation matrix was specified as,

$$R = \begin{bmatrix} \cos(\theta) & -\sin(\theta) \\ \sin(\theta) & \cos(\theta) \end{bmatrix}, \tag{3}$$

where θ is the amount (in radians) the data are to be rotated. We specified θ as the negative arc-tangent of c (as applying the arc-tangent function to the tangent of a triangle (the tangent being equivalent to the slope of a line) produces the angle in radians). For each species, we applied the rotation matrix to logged body mass (LM) and logged wing length (LW), to reproject the data onto new axes (Extended Data Fig. 2),

$$\begin{bmatrix} x' \\ y' \end{bmatrix} = R \begin{bmatrix} LM \\ LW \end{bmatrix}. \tag{4}$$

These reprojected data (x' and y') were standardized within species (centred and divided by the standard deviation) to create two relative indices (SI and WI) that represent the overall size of the individual and the degree to which wing length deviates from its expected value given the body mass of the individual, respectively,

$$\frac{x'_{ik} - \overline{x'_{k}}}{\sigma_{xr_{k}}} = SI_{ik}$$

$$\frac{y'_{ik} - \overline{y'_{k}}}{\sigma_{yr_{k}}} = WI_{ik}$$
(5)

where $\overrightarrow{x'}$ and $\overrightarrow{y'}$ represent the mean and $\sigma_{x'}$ and $\sigma_{y'}$ represent the standard deviation of x' and y', respectively, for each species, k, and i represents each bird capture. This approach allowed us to account for the expected nonlinear relationship among these traits when assessing spatiotemporal change and provides a means by which to assess morphological deviations from an expectation that is rooted in scaling theory and validated with empirical estimates ¹⁴. Because of this, we were able to make inference on changes in the overall size and wingyness of these

species directly, without the use of additional metrics. This approach also accounts for variation in morphological change among species of different sizes (modelling proportional rather than absolute change), as these indices are standardized within each species. SI values were closely correlated with logged mass (mean correlation coefficient across species = 0.99, range 0.98–1). WI values showed a strong correlation to logged wing length (mean correlation coefficient across species = 0.75, range 0.49–0.88), although not as strong as the relationship between SI and logged mass.

Morphology as a function of time, latitude and elevation

We used a hierarchical Bayesian approach to determine how SI and WI varied within species as a function of time, latitude and elevation. We fit separate models for each index, that were identical in structure. In each case, the index (y_{IDX}) for capture i, at banding station j, for species k was modelled as t-distributed, as a linear function of time,

$$y_{\text{IDX}_{ijk}} \sim t(v_{\text{IDX}}, \mu_{\text{IDK}_{ijk}}, \sigma_{\text{IDX}_k}),$$

$$\mu_{\text{IDX}_{ijk}} = \alpha_{\text{IDX}_k} + \beta_{\text{IDX}_{ik}} \times \text{year}_{ijk} + \xi_{\text{IDX}_{ik}},$$
(6)

where $\alpha_{\rm IDX}$ is the species-level intercept term, $\beta_{\rm IDX}$ is the effect of year on the response variable, $\xi_{\rm IDX}$ is the species-station intercept term, $\sigma_{\rm IDX}$ is the species-specific process error, $v_{\rm IDX}$ represents the degrees of freedom, controlling the normality of the distribution (resulting in a Cauchy distribution when $v_{\rm IDX}=1$ and approaching a normal distribution as $v_{\rm IDX}$ approaches infinity) and the IDX subscript denotes the association of that parameter with this model (to help distinguish these parameters from those in other models). The degrees of freedom parameter of the t-distribution allows for additional flexibility (compared with the normal distribution) in modelling the structure of the residuals (for instance when there are 'extreme observations' 70). Parameter $\alpha_{\rm IDX}$ was modelled as normally distributed,

$$\alpha_{\text{IDX}_k} \sim N(\mu_{\alpha_{\text{IDX}}}, \sigma_{\alpha_{\text{IDX}}}),$$
 (7)

where $\mu_{\alpha_{\rm IDX}}$ and $\sigma_{\alpha_{\rm IDX}}$ represent the mean and standard deviation of $\alpha_{\rm IDX}$ across all species, respectively. Parameter $\beta_{\rm IDX}$ was modelled as normally distributed,

$$\beta_{\text{IDX}_{ik}} \sim N(\eta_{\text{IDX}_k}, \sigma_{\beta_{\text{IDX}}}),$$
 (8)

where η_{IDX} represents the mean effect of year on the response for each species and $\sigma_{\beta_{\text{IDX}}}$ represents the process error. Parameter σ_{IDX} was modelled as half-normal (normal but with support only over positive values),

$$\sigma_{\text{IDX}_k} \sim \text{HN}(\tau_{\sigma_{\text{IDX}}}, \kappa_{\sigma_{\text{IDX}}}),$$
 (9)

where au_{olio} and au_{olio} represent the mean and standard deviation of σ_{IDX} , respectively. Process error was modelled hierarchically, as the degree to which these explanatory variables explain that variation in the data may vary by species. Parameter η_{IDX} was modelled as normally distributed,

$$\eta_{\text{IDX}_k} \sim N(\mu_{\eta_{\text{IDX}}}, \sigma_{\eta_{\text{IDX}}}),$$
(10)

where $\mu_{\eta_{\rm IDX}}$ and $\sigma_{\eta_{\rm IDX}}$ represent the mean and standard deviation of $\eta_{\rm IDX}$ across all species, respectively. The species-station intercept term, $\xi_{\rm IDX}$, was modelled as a linear function of latitude and elevation,

$$\begin{split} \xi_{\mathrm{IDX}_{jk}} &\sim \mathcal{N}(\mu_{\xi_{\mathrm{IDX}_{jk}}}, \sigma_{\xi_{\mathrm{IDX}_{k}}}) \\ \mu_{\xi_{\mathrm{IDX}_{jk}}} &= \gamma_{\mathrm{IDX}_{k}} \times \mathrm{lat}_{jk} + \theta_{\mathrm{IDX}_{k}} \times \mathrm{elev}_{jk} \\ \left[\begin{array}{c} \gamma_{\mathrm{IDX}_{k}} \\ \theta_{\mathrm{IDX}_{k}} \end{array} \right] &\sim \mathrm{MVN} \left(\begin{bmatrix} \mu_{\gamma_{\mathrm{IDX}}} \\ \mu_{\theta_{\mathrm{IDX}}} \end{bmatrix}, \Sigma_{\mathrm{IDX}} \right), \end{split} \tag{11}$$

where γ_{IDX} is the species-specific effect of latitude (lat) on ξ_{IDX} on θ_{IDX} is the species-specific effect of elevation (elev) on ξ_{IDX} and $\sigma_{\xi_{\text{IDX}}}$ is the species-specific process error. Parameters γ_{IDX} and θ_{IDX} were modelled as multivariate normal, with means $\mu_{\gamma_{\text{IDX}}}$ and $\mu_{\theta_{\text{IDX}}}$, respectively, and covariance Σ_{IDX} (a 2 × 2 covariance matrix). Parameter $\sigma_{\xi_{\text{IDX}}}$ was modelled as half-normal

$$\sigma_{\xi_{\text{IDX}_{k}}} \sim \text{HN}(\tau_{\sigma_{\xi_{\text{IDX}}}}, \kappa_{\sigma_{\xi_{\text{IDX}}}}),$$
 (12)

where $\tau_{\sigma_{\xi_{mn}}}$ and $\kappa_{\sigma_{\xi_{mn}}}$ represent the mean and standard deviation of $\sigma_{\xi_{nn'}}$ respectively. We fit all Bayesian models in this study using the R package 'rstan'⁷¹ to interface with Stan⁷² in R (ref. ⁶⁶). R package 'MCMCvis'⁷³ was used to summarize, visualize and manipulate all Bayesian model output. General data manipulation and processing was done using the 'tidyverse' family of R packages⁷⁴. For each model, we ran four chains for 8,000 iterations each with a warmup of 4,000 iterations. For all models. Rhat ≤ 1.01 and the number of effective samples was >400 for all parameters. No models had divergent transitions⁷². Weakly informative priors were given for all parameters. Stan files with full model specifications can be found in the archived Github repository associated with this manuscript. For each parameter that required a prior, the overlap between the prior and posterior distribution was visualized and calculated to ensure that the priors were not having an outsized effect on the posterior distribution. Graphical posterior predictive checks were used to check that data generated by the model were similar to the data used to fit the model⁷⁵. Data simulated from the posterior predictive distribution were similar to the observed data (Supplementary Fig. 1).

For all model results in the main text, we present posterior mean estimates for parameters as well as the 89% CI, following ref. 76 . The choice of 89% is arbitrary but serves to quantify parameter uncertainty while avoiding any suggestion that Bayesian credible intervals are analogous to tests of statistical significance (as might be assumed if using 95% cutoffs). For each parameter, we also present the probability that a given parameter is positive (calculated as the proportion of the posterior that is >0) as $P({\rm PARAMETER}>0)$, or negative (the proportion of the posterior that is <0) as $P({\rm PARAMETER}<0)$. Scenarios in which $P({\rm PARAMETER}>0)$ or $P({\rm PARAMETER}<0)$ are near 0.5 indicate that a positive relationship is equally likely as a negative relationship.

To create species maps for Figs. 2c, 3c and 4b, we used range maps obtained from ref. 77. Estimated effects of latitude and elevation were used to predict values for SI and WI across the range of these species. For Fig. 3c, we excluded all areas >2,000 m when making predictions for the SI for red-eyed vireo (*V. olivaceus*). This was done to avoid making predictions outside the elevational range of this species in the Rocky Mountains—the range maps used did not incorporate elevation information and 2,000 m is the elevational range limit for this species⁷⁸.

Body size as a function of temporal variation in temperature

To quantify how intraspecific variation in size across time is influenced by temperature, we modelled SI as a function MT (May–July maximum temperature at each station). The response variable (y_{TVT}) for capture i, banding station j and species k was modelled as t-distributed, as a function of MT,

$$y_{\text{TVT}_{ijk}} \sim t(\nu_{\text{TVT}}, \mu_{\text{TVT}_{ijk}}, \sigma_{\text{TVT}_k})$$

$$\mu_{\text{TVT}_{ijk}} = \alpha_{\text{TVT}_{jk}} + \beta_{\text{TVT}_{jk}} \times \text{MT}_{ijk},$$
(13)

where α_{TVT} is the species-station-specific intercept term, β_{TVT} is the species-station-specific effect of temperature on the response variable, σ_{TVT} is the species-specific process error, ν_{TVT} represents the degrees of freedom and the TVT subscript denotes the association of that parameter with this model. Parameter α_{TVT} was modelled normally distributed, as a function of MST (deviations of May–July

maximum temperature from species-specific range-wide temperature at each station).

$$\alpha_{\text{TVT}_{jk}} \sim N(\mu_{\alpha_{\text{TVT}_{jk}}}, \sigma_{\alpha_{\text{TVT}}})$$

$$\mu_{\alpha_{\text{TVT}_{jk}}} = \rho_{\text{TVT}_k} + \zeta_{\text{TVT}_k} \times \text{MST}_{jk}$$

$$\begin{bmatrix} \rho_{\text{TVT}_k} \\ \zeta_{\text{TVT}_k} \end{bmatrix} \sim \text{MVN} \left(\begin{bmatrix} \mu_{\rho_{\text{TVT}}} \\ \mu_{\zeta_{\text{TVT}}} \end{bmatrix}, \Sigma_{\alpha_{\text{TVT}}} \right)$$
(14)

where ρ_{TVT} is the species-specific intercept term, ζ_{TVT} is the species-specific effects of MST on α_{TVT} and $\sigma_{\alpha_{\text{TVT}}}$ represents the process error. Parameters ρ_{TVT} and ζ_{TVT} were modelled as multivariate normal, with means $\mu_{\rho_{\text{TVT}}}$ and $\mu_{\zeta_{\text{TVT}}}$ respectively, and covariance $\Sigma_{\alpha_{\text{TVT}}}$ (a 2 × 2 covariance matrix). Parameter β_{TVT} was similarly modelled as a function of MST.

$$\beta_{\text{TVT}_{jk}} \sim N(\mu_{\beta_{\text{TVT}_{jk}}}, \sigma_{\beta_{\text{TVT}}})$$

$$\mu_{\beta_{\text{TVT}_{jk}}} = \gamma_{\text{TVT}_{k}} + \theta_{\text{TVT}_{k}} \times \text{MST}_{jk}$$

$$\begin{bmatrix} \gamma_{\text{TVT}_{k}} \\ \theta_{\text{TVT}_{k}} \end{bmatrix} \sim \text{MVN} \left(\begin{bmatrix} \mu_{\gamma_{\text{TVT}}} \\ \mu_{\theta_{\text{DVT}}} \end{bmatrix}, \Sigma_{\beta_{\text{TVT}}} \right)$$
(15)

Both the intercept (α_{TVT}) and slope (β_{TVT}) at each species-station were modelled as a function of mean station temperature because both the overall size and the effect of temporal variation in temperature might be expected to vary across this gradient. Parameter σ_{TVT} was modelled as half-normal,

$$\sigma_{\text{TVT}_k} \sim \text{HN}(\tau_{\sigma_{\text{TVT}}}, \kappa_{\sigma_{\text{TVT}}}),$$
 (16)

where $\tau_{\sigma_{\text{TVT}}}$ and $\kappa_{\sigma_{\text{TVT}}}$ represent the mean and standard deviation of σ_{TVT} , respectively.

We fit three identical versions of this model, using temperature data in the year that the morphological data were collected (lag 0), as well as temperature 1 year (lag 1) and 2 years (lag 2) before data collection, to explore the effect of temperature on morphology (that is, the effect of temperature in year t, t-1 and t-2 on morphology in year t) during the potential hatching summer and subsequent summers and to account for the uncertainty and variability in the ages of these birds (all of which were known to be adults). For each model, we ran four chains for 6,000 iterations each with a warmup of 3,000 iterations.

Body size as a function of spatial variation in temperature

To quantify how intraspecific variation in size across space is influenced by temperature, we modelled SI as a function of MT (mean May–July maximum temperature at each station across all years). The response variable (y_{SVT}) for capture i, banding station j and species k was modelled as t-distributed,

$$y_{\text{SVT}_{ijk}} \sim t(v_{\text{SVT}}, \mu_{\text{SVT}_{ijk}}, \sigma_{\text{SVT}_k})$$

$$\mu_{\text{SVT}_{ijk}} = \alpha_{\text{SVT}_k} + \xi_{\text{SVT}_{ik}},$$
(17)

where α_{SVT} is the species-specific intercept term, ξ_{SVT} is the species-station-specific intercept, σ_{SVT} is the species-specific processes error, ν_{SVT} represents the degrees of freedom and SVT denotes the association of each parameter with this model. Parameter α_{SVT} was modelled as normally distributed,

$$\alpha_{\text{SVT}_k} \sim N(\mu_{\alpha_{\text{SVT}}}, \sigma_{\alpha_{\text{SVT}}}),$$
(18)

where μ_{α} and σ_{α} represent the mean and standard deviation of $\alpha_{\rm SVT}$, respectively. Parameter $\xi_{\rm SVT}$ was modelled as normally distributed, as a function of MT,

$$\xi_{\text{SVT}_{jk}} \sim N(\mu_{\xi_{\text{SVT}_{jk}}}, \sigma_{\xi_{\text{SVT}}})$$

$$\mu_{\xi_{\text{SVT}_{jk}}} = \beta_{\text{SVT}_{k}} \times \text{MT},$$
(19)

where β_{SVT_k} is the species-specific effect of MT and $\sigma_{\xi_{\text{SVT}}}$ is the process error. Parameter β_{SVT} was modelled as normally distributed,

$$\beta_{\text{SVT}_k} \sim N(\mu_{\beta_{\text{SVT}}}, \sigma_{\beta_{\text{SVT}}}),$$
 (20)

where $\mu_{\beta_{SVT}}$ and $\sigma_{\beta_{SVT}}$ represent the mean and standard deviation of β_{SVT} , respectively. We ran four chains for this model for 8,000 iterations each with a warmup of 4,000 iterations.

To assess how responses to temperature varied across species, we modelled the species-specific effect of spatial variation of temperature on SI ($\widehat{\beta_{\text{SVT}}}$; the posterior mean of β_{SVT} (equation (19)), derived from the above model) and associated uncertainty as a function of ST (mean cross-station temperature within each species' range). Parameter $\widehat{\beta_{\text{SVT}}}$ was modelled as normally distributed, with mean π_{SR} and standard deviation $\sigma_{\widehat{\beta_{\text{SVT}}}}$ (the posterior standard deviation of β_{SVT} (equation (19)), derived from the above model),

$$\widehat{\beta_{\text{SVT}_k}} \sim N\left(\pi_{\text{SR}_k}, \sigma_{\widehat{\beta_{\text{SVT}_k}}}\right),$$
 (21)

where SR denotes the association of each parameter with this model. In this way, the uncertainty in the species-specific estimates of the spatial temperature effect is propagated through these analyses. Parameter π_{SVT} was modelled as multivariate normal, as a linear function of ST, in a manner that accounts for the phylogenetic non-independence between species (following refs. ^{79,80}),

$$\pi_{\mathsf{SR}_k} \sim \mathsf{MVN}\left(\mu_{\pi_{\mathsf{SR}_k}}, \Sigma_{\mathsf{SR}} \times \sigma_{\pi_{\mathsf{SR}}}\right)$$

$$\mu_{\pi_{\mathsf{SR}_k}} = \gamma_{\mathsf{SR}} + \theta_{\mathsf{SR}} \times \mathsf{ST}_k$$

$$\Sigma_{\mathsf{SR}} = \lambda_{\mathsf{SR}} \times \Sigma_{\mathsf{dis}} + (1 - \lambda_{\mathsf{SR}}) \times I,$$
(22)

where y_{SR} is the intercept term, θ_{SR} is the effect of ST on the response variable and $\sigma_{\pi_{SR}}$ is the process error. Parameter Σ_{dis} is a phylogenetic covariance matrix, standardized such that the diagonal elements have a value of 1. The off-diagonal elements of Σ_{dis} describe the pair-wise phylogenetic distances between the 105 species included in this study. The phylogenetic covariance matrix was calculated from a consensus phylogenetic tree (using the 'phytools' package^{SI} in R) on the basis of 100 trees for the species of interest obtained from BirdTree⁶⁷. Parameter λ_{SR} is Pagel's lambda^{S2}, which represents the degree to which phylogenetic relatedness contributes to variation in π_{SR} , where values near 0 (the lower bound of the parameter) indicate low phylogenetic signal and values near 1 (the upper bound of the parameter) correspond to variation following a Brownian motion model of evolution of and lis an identity matrix. We ran this model for 1,000 iterations with a warmup of 500 iterations.

Back-transformation of effect sizes to trait space

Steps outlined by equations (1)–(5) were implemented in reverse, to calculate the response of absolute morphological measurements (body mass and wing length) to variation over time, latitude and elevation, using posterior estimates for the effects of these predictors on SI and WI. That is, for each species the effect sizes (posterior estimates) of these covariates on SI and WI were multiplied by the standard deviation of x' and y' ($a_{x'}$ and $a_{y'}$ respectively),

$$\phi_{x'_k} = \phi_{SI_k} \times \sigma_{x'_k}
\phi_{y'_k} = \phi_{WI_k} \times \sigma_{y'_k},$$
(23)

where ϕ_{SI} and ϕ_{WI} are the effect of a given covariate on SI and WI, respectively, for each species (k) and ϕ_{xv} , and ϕ_{yv} , represent the unstandardized effects of the covariate for each species. Parameters ϕ_{xv} and ϕ_{yv} , were then rotated using the transpose of R (equation (3)),

$$\begin{bmatrix} \phi_{\mathsf{LM}_k} \\ \phi_{\mathsf{LW}_k} \end{bmatrix} = R^T \begin{bmatrix} \phi_{x\prime_k} \\ \phi_{y\prime_k} \end{bmatrix},\tag{24}$$

where ϕ_{LM} and ϕ_{LW} represent the effect of a given covariate on the logged absolute morphological metrics, LM (logged mass) and LW (logged wing length), for each species. This transformation has the effect of rotating data in the opposite direction of the rotation performed in equation (4). Since ϕ_{LM} and ϕ_{LW} represent an effect size in log space, when exponentiated, these metrics represent the multiplicative change in (unlogged) mass and wing length for each one-unit change in a given covariate. Subtracting one from this value and multiplying by 100 gives the percentage change in that metric. To determine the percentage change in mass (ω_{M}) and wing length (ω_{W}) over the temporal, latitudinal and elevational range at which data were collected for each species, we exponentiated the product of ϕ_{LM} and L (for mass) and the product of ϕ_{LW} and L (for wing length), subtracted one and multiplied by 100,

$$\begin{split} &\omega_{\mathrm{M}_{\mathrm{COV}_k}} = \left(\left(e^{\phi_{\mathrm{LM}_k} \times L_k} \right) - 1 \right) \times 100 \\ &\omega_{\mathrm{W}_{\mathrm{COV}_k}} = \left(\left(e^{\phi_{\mathrm{LW}_k} \times L_k} \right) - 1 \right) \times 100, \end{split} \tag{25}$$

where L represents the total number of covariate units (that is, 30 years, the latitudinal range in degrees for a given species or the elevational range in metres for a given species) and COV represents time ($\omega_{\rm M_{TIME}}$ or $\omega_{\rm W_{TIME}}$), latitude ($\omega_{\rm M_{LAT}}$ or $\omega_{\rm W_{LAT}}$) or elevation ($\omega_{\rm M_{ELEV}}$ or $\omega_{\rm W_{ELEV}}$). This was done at each iteration of the posterior for the estimated effect of year ($\beta_{\rm IDX}$; equation (6)), latitude ($\gamma_{\rm IDX}$; equation (11)) and elevation ($\theta_{\rm IDX}$; equation (11)), providing a posterior distribution for $\omega_{\rm M_{COV}}$ and $\omega_{\rm W_{COV}}$ are calculated the mean of $\omega_{\rm M_{COV}}$ and $\omega_{\rm W_{COV}}$ arcross all species at each posterior iteration, represented by $\mu_{\omega_{\rm M_{COV}}}$ and $\mu_{\omega_{\rm W_{COV}}}$, respectively,

$$\mu_{\omega_{\text{M}_{\text{COV}}}} = \frac{\sum_{k=1}^{N} \omega_{\text{M}_{\text{COV}_k}}}{N}$$

$$\mu_{\omega_{\text{W}_{\text{COV}}}} = \frac{\sum_{k=1}^{N} \omega_{\text{W}_{\text{COV}_k}}}{N},$$
(26)

where N is the number of species.

Rate of morphological change

To compare the observed rates of phenotypic change in this study to observed rates of evolutionary change in other taxa, we calculated change in logged mass in terms of haldanes (h),

$$h = \frac{\left(\frac{x_2}{\varsigma_p}\right) - \left(\frac{x_1}{\varsigma_p}\right)}{g},\tag{27}$$

where x_2 and x_1 are the mean values for a morphological trait of interest at two time points, s_p is the standard deviation of the traits (pooled across time) and g is the number of generations that are likely to have occurred between the two time points⁸³. This measure, first proposed by ref. ⁸⁴, represents the magnitude of phenotypic change in standard deviations per generation.

For each species, we predicted logged mass at the beginning (x_1) and end (x_2) of the 30-yr study period by subtracting and adding $\phi_{\text{LM}_{\text{TIME}}} \times 15$ (where $\phi_{\text{LM}_{\text{TIME}}}$ is from equation (24), representing change in logged mass per year), respectively, from mean logged mass. We calculated the within-population standard deviation across all years at each station and took the mean value of this standard deviation across stations (s_p) for each species. We used information on generation length from ref. Standard to calculate the number of generations (generation length/30) for a particular species over this time period (g).

Previous work has suggested that rates of evolutionary change of |h| = 0.1-0.3 standard deviations per generation are rapid ⁸⁶ and that the maximal rate of phenotypic change that can be sustained indefinitely

is -0.1 phenotypic standard deviations per generation⁸⁷. For all species in this study, |h| < 0.1. Rates of phenotypic change were similar to those observed in other taxa undergoing anthropogenic disturbance (Extended Data Fig. 9)⁸⁸.

Reporting summary

Further information on research design is available in the Nature Research Reporting Summary linked to this article.

Data availability

Data from the MAPS programme are curated and managed by The Institute for Bird Populations and were queried from the MAPS database on 16 October 2019. MAPS data used here are available on Dryad (https://doi.org/10.5068/D1DT2T).

Code availability

All code used to produce analyses are freely available on Github (https://github.com/caseyyoungflesh/MAPS_morph_changes) and archived on Zenodo (https://doi.org/10.5281/zenodo.6977666).

References

- Dehling, D. M., Jordano, P., Schaefer, H. M., Böhning-Gaese, K. & Schleuning, M. Morphology predicts species' functional roles and their degree of specialization in plant–frugivore interactions. *Proc. R. Soc. B* 283, 20152444 (2016).
- Grant, P. R. Inheritance of size and shape in a population of Darwin's finches, Geospiza conirostris. Proc. R. Soc. Lond. B 220, 219–236 (1983).
- 3. Des Roches, S. et al. The ecological importance of intraspecific variation. *Nat. Ecol. Evol.* **2**, 57–64 (2018).
- Bergmann, C. Über die verhältnisse der wärmeökonomie der thiere zu ihrer grösse. Gött. Stud. 3, 595–708 (1847).
- 5. Allen, J. A. The influence of physical conditions in the genesis of species. *Radic. Rev.* **1**, 108–140 (1877).
- Altshuler, D. L. & Dudley, R. The physiology and biomechanics of avian flight at high altitude. *Integr. Comp. Biol.* 46, 62–71 (2006).
- 7. Teplitsky, C. & Millien, V. Climate warming and Bergmann's rule through time: is there any evidence? *Evol. Appl.* **7**, 156–168 (2014).
- Gardner, J. L., Peters, A., Kearney, M. R., Joseph, L. & Heinsohn, R. Declining body size: a third universal response to warming? Trends Ecol. Evol. 26, 285–291 (2011).
- Yom-Tov, Y., Yom-Tov, S., Wright, J., Thorne, C. J. R. & Du Feu, R. Recent changes in body weight and wing length among some British passerine birds. Oikos 112, 91–101 (2006).
- Van Buskirk, J., Mulvihill, R. S. & Leberman, R. C. Declining body sizes in North American birds associated with climate change. Oikos 119, 1047–1055 (2010).
- Weeks, B. C. et al. Shared morphological consequences of global warming in North American migratory birds. *Ecol. Lett.* 23, 316–325 (2020).
- Rosenberg, K. V. et al. Decline of the North American avifauna. Science 366, 120–124 (2019).
- DeSante, D. F., Saracco, J. F., O'Grady, D. R., Burton, K. M. & Walker, B. L. Methodological considerations of the Monitoring Avian Productivity and Survivorship (MAPS) program. Stud. Avian Biol. 29, 28–45 (2004).
- West, G. B., Brown, J. H. & Enquist, B. J. A general model for the origin of allometric scaling laws in biology. *Science* 276, 122–126 (1997).
- Jirinec, V. et al. Morphological consequences of climate change for resident birds in intact Amazonian rainforest. Sci. Adv. 7, eabk1743 (2021).
- Dubiner, S. & Meiri, S. Widespread recent changes in morphology of Old World birds, global warming the immediate suspect. *Glob. Ecol. Biogeogr.* 31, 791–801 (2022).

- Ballinger, M. A. & Nachman, M. W. The contribution of genetic and environmental effects to Bergmann's rule and Allen's rule in house mice. Am. Nat. https://doi.org/10.1086/719028 (2022).
- Andrew, S. C., Hurley, L. L., Mariette, M. M. & Griffith, S. C. Higher temperatures during development reduce body size in the zebra finch in the laboratory and in the wild. *J. Evol. Biol.* 30, 2156–2164 (2017).
- Siepielski, A. M. et al. No evidence that warmer temperatures are associated with selection for smaller body sizes. *Proc. R. Soc. B* 286, 20191332 (2019).
- Salewski, V., Siebenrock, K.-H., Hochachka, W. M., Woog, F. & Fiedler, W. Morphological change to birds over 120 years is not explained by thermal adaptation to climate change. *PLoS ONE* 9, e101927 (2014).
- Riddell, E. A., Iknayan, K. J., Wolf, B. O., Sinervo, B. & Beissinger, S. R. Cooling requirements fueled the collapse of a desert bird community from climate change. *Proc. Natl Acad. Sci. USA* 116, 21609–21615 (2019).
- Pecl, G. T. et al. Biodiversity redistribution under climate change: impacts on ecosystems and human well-being. Science 355, eaai9214 (2017).
- Futuyma, D. J. Evolutionary constraint and ecological consequences. Evolution 64, 1865–1884 (2010).
- Murren, C. J. et al. Constraints on the evolution of phenotypic plasticity: limits and costs of phenotype and plasticity. *Heredity* 115, 293–301 (2015).
- Rollinson, C. R. et al. Working across space and time: nonstationarity in ecological research and application. Front. Ecol. Environ. 19, 66–72 (2021).
- Riemer, K., Guralnick, R. P. & White, E. P. No general relationship between mass and temperature in endothermic species. *eLife* 7, e27166 (2018).
- Ryding, S., Klaassen, M., Tattersall, G. J., Gardner, J. L. & Symonds, M. R. Shape-shifting: changing animal morphologies as a response to climatic warming. *Trends Ecol. Evol.* 36, 1036–1048 (2021).
- Baldwin, M. W., Winkler, H., Organ, C. L. & Helm, B. Wing pointedness associated with migratory distance in common-garden and comparative studies of stonechats (Saxicola torquata). J. Evol. Biol. 23, 1050–1063 (2010).
- Förschler, M. I. & Bairlein, F. Morphological shifts of the external flight apparatus across the range of a passerine (Northern Wheatear) with diverging migratory behaviour. *PLoS ONE* 6, e18732 (2011).
- Macpherson, M. P., Jahn, A. E. & Mason, N. A. Morphology of migration: associations between wing shape, bill morphology and migration in kingbirds (*Tyrannus*). *Biol. J. Linn. Soc.* 135, 71–83 (2022).
- 31. Newton, I. The Migration Ecology of Birds (Elsevier, 2010).
- Clegg, S. M., Kelly, J. F., Kimura, M. & Smith, T. B. Combining genetic markers and stable isotopes to reveal population connectivity and migration patterns in a neotropical migrant, Wilson's warbler (Wilsonia pusilla). Mol. Ecol. 12, 819–830 (2003).
- 33. Bell, C. P. Leap-frog migration in the fox sparrow: minimizing the cost of spring migration. *Condor* **99**, 470–477 (1997).
- Billerman, S., Keeney, B., Rodewald, P. & Schulenberg, T. (eds) Birds of the World (Cornell Laboratory of Ornithology, 2020).
- Desrochers, A. Morphological response of songbirds to 100 years of landscape change in North America. *Ecology* 91, 1577–1582 (2010).
- Swaddle, J. P. & Lockwood, R. Morphological adaptations to predation risk in passerines. J. Avian Biol. 29, 172–176 (1998).
- Chown, S. L. & Klok, C. J. Altitudinal body size clines: latitudinal effects associated with changing seasonality. *Ecography* 26, 445–455 (2003).

- 38. Hsiung, A. C., Boyle, W. A., Cooper, R. J. & Chandler, R. B. Altitudinal migration: ecological drivers, knowledge gaps, and conservation implications: animal altitudinal migration review. *Biol. Rev.* **93**, 2049–2070 (2018).
- Barras, A. G., Liechti, F. & Arlettaz, R. Seasonal and daily movement patterns of an alpine passerine suggest high flexibility in relation to environmental conditions. *J. Avian Biol.* 52, jav.02860 (2021).
- Spence, A. R. & Tingley, M. W. Body size and environment influence both intraspecific and interspecific variation in daily torpor use across hummingbirds. Funct. Ecol. 35, 870–883 (2021).
- 41. Moreau, R. E. Variation in the western Zosteropidae (Aves). *Bull. Br. Mus. Nat. Hist. Zool.* **4**, 311–433 (1957).
- 42. Hamilton, T. H. The adaptive significances of intraspecific trends of variation in wing length and body size among bird species. *Evolution* **15**, 180–194 (1961).
- 43. Hodkinson, I. D. Terrestrial insects along elevation gradients: species and community responses to altitude. *Biol. Rev.* **80**, 489–513 (2005).
- 44. Feinsinger, P., Colwell, R. K., Terborgh, J. & Chaplin, S. B. Elevation and the morphology, flight energetics, and foraging ecology of tropical hummingbirds. *Am. Nat.* **113**, 481–497 (1979).
- Aldrich, J. W. Ecogeographical Variation in Size and Proportions of Song Sparrows (Melospiza melodia) (American Ornithological Society, 1984).
- 46. Sun, Y. et al. The role of climate factors in geographic variation in body mass and wing length in a passerine bird. *Avian Res.* **8**, 1 (2017).
- Des Roches, S., Pendleton, L. H., Shapiro, B. & Palkovacs, E. P. Conserving intraspecific variation for nature's contributions to people. *Nat. Ecol. Evol.* 5, 574–582 (2021).
- 48. McKechnie, A. E. & Wolf, B. O. Climate change increases the likelihood of catastrophic avian mortality events during extreme heat waves. *Biol. Lett.* **6**, 253–256 (2010).
- Conradie, S. R., Woodborne, S. M., Cunningham, S. J. & McKechnie, A. E. Chronic, sublethal effects of high temperatures will cause severe declines in southern African arid-zone birds during the 21st century. *Proc. Natl Acad. Sci. USA* 116, 14065– 14070 (2019).
- Radchuk, V. et al. Adaptive responses of animals to climate change are most likely insufficient. Nat. Commun. 10, 3109 (2019).
- Riddell, E. A. et al. Exposure to climate change drives stability or collapse of desert mammal and bird communities. Science 371, 633–636 (2021).
- 52. Tingley, M. W., Monahan, W. B., Beissinger, S. R. & Moritz, C. Birds track their Grinnellian niche through a century of climate change. *Proc. Natl Acad. Sci. USA* **106**, 19637–19643 (2009).
- 53. Youngflesh, C. et al. Migratory strategy drives species-level variation in bird sensitivity to vegetation green-up. *Nat. Ecol. Evol.* **5**, 987–994 (2021).
- 54. Blueweiss, L. et al. Relationships between body size and some life history parameters. *Oecologia* **37**, 257–272 (1978).
- 55. Kleiber, M. Body size and metabolic rate. *Physiol. Rev.* 27, 511–541 (1947).
- 56. Yodzis, P. & Innes, S. Body size and consumer-resource dynamics. *Am. Nat.* **139**, 1151–1175 (1992).
- 57. Prum, R. O. Interspecific social dominance mimicry in birds: social mimicry in birds. *Zool. J. Linn.* Soc. **172**, 910–941 (2014).
- 58. Pyle, P. Identification Guide to North American Birds: A Compendium of Information on Identifying, Ageing, and Sexing 'Near-Passerines' and Passerines in the Hand (Slate Creek Press, 1997).
- Leys, C., Ley, C., Klein, O., Bernard, P. & Licata, L. Detecting outliers: do not use standard deviation around the mean, use absolute deviation around the median. J. Exp. Soc. Psychol. 49, 764–766 (2013).

- 60. Danielson, J. J. & Gesch, D. B. Global Multi-Resolution Terrain Elevation Data 2010 (GMTED2010) (US Geological Survey, 2011).
- Thornton, M. M. et al. Daymet: Daily Surface Weather Data on a 1-km Grid for North America, Version 4 (ORNL Distributed Active Archive Center, 2020).
- 62. Greenewalt, C. H. The flight of birds: the significant dimensions, their departure from the requirements for dimensional similarity, and the effect on flight aerodynamics of that departure. *Trans. Am. Philos. Soc.* **65**, 1–67 (1975).
- 63. Longo, G. & Montévil, M. Perspectives on Organisms: Biological Time, Symmetries, and Singularities (Springer, 2014).
- 64. Harvey, P. H. in Scaling in Biology (eds Brown, J. H. & West, G. B.) 253–265 (Oxford Univ. Press, 2000).
- Orme, D. et al. The caper package: comparative analysis of phylogenetics and evolution in R. R package version 5 (2013).
- 66. R Core Team. R: A Language and Environment for Statistical Computing (R Foundation for Statistical Computing, 2021).
- Jetz, W., Thomas, G. H., Joy, J. B., Hartmann, K. & Mooers, A. O. The global diversity of birds in space and time. *Nature* 491, 444–448 (2012).
- 68. Nudds, R. L., Kaiser, G. W. & Dyke, G. J. Scaling of avian primary feather length. *PLoS ONE* **6**, e15665 (2011).
- 69. Nudds, R. Wing-bone length allometry in birds. J. Avian Biol. 38, 515–519 (2007).
- Anderson, S. C., Branch, T. A., Cooper, A. B. & Dulvy, N. K. Black-swan events in animal populations. *Proc. Natl Acad. Sci.* USA 114, 3252–3257 (2017).
- Stan Modeling Language Users Guide and Reference Manual, Version 2.18.0 (Stan Development Team, 2018); http://mc-stan.org
- 72. Carpenter, B. et al. Stan: a probabilistic programming language. *J. Stat. Softw.* **76**, 1–32 (2017).
- 73. Youngflesh, C. MCMCvis: tools to visualize, manipulate, and summarize MCMC output. *J. Open Source Softw.* **3**, 640 (2018).
- 74. Wickham, H. et al. Welcome to the Tidyverse. J. Open Source Softw. 4, 1686 (2019).
- Gabry, J., Simpson, D., Vehtari, A., Betancourt, M. & Gelman, A. Visualization in Bayesian workflow. J. R. Stat. Soc. A 182, 389–402 (2019).
- 76. McElreath, R. Statistical Rethinking: A Bayesian Course with Examples in R and Stan (Chapman and Hall/CRC, 2018).
- Data Zone (BirdLife International, 2019); http://datazone.birdlife. org/species/requestdis
- Cramp, S. & Brooks, D. Handbook of the Birds of Europe, the Middle East and North Africa. The Birds of the Western Palearctic, Vol. VI. Warblers (Oxford Univ. Press, 1992).
- Che-Castaldo, J., Che-Castaldo, C. & Neel, M. C. Predictability of demographic rates based on phylogeny and biological similarity. Conserv. Biol. 32, 1290–1300 (2018).
- Villemereuil, P., de, Wells, J. A., Edwards, R. D. & Blomberg, S. P. Bayesian models for comparative analysis integrating phylogenetic uncertainty. *BMC Evol. Biol.* 12, 102 (2012).
- 81. Revell, L. J. phytools: an R package for phylogenetic comparative biology (and other things). *Methods Ecol. Evol.* **3**, 217–223 (2012).
- 82. Pagel, M. Inferring the historical patterns of biological evolution. *Nature* **401**, 877–884 (1999).
- 83. Hendry, A. P. & Kinnison, M. T. Perspective: the pace of modern life: measuring rates of contemporary microevolution. *Evolution* **53**, 1637–1653 (1999).

- 84. Gingerich, P. Rates of evolution: effects of time and temporal scaling. *Science* **222**. 159–162 (1983).
- 85. Bird, J. P. et al. Generation lengths of the world's birds and their implications for extinction risk. *Conserv. Biol.* **34**, 1252–1261 (2020).
- Gingerich, P. D. Rates of evolution. *Annu. Rev. Ecol. Evol. Syst.* 40, 657–675 (2009).
- 87. Bürger, R. & Lynch, M. Evolution and extinction in a changing environment: a quantitative-genetic analysis. *Evolution* **49**, 151–163 (1995).
- 88. Hendry, A. P., Farrugia, T. J. & Kinnison, M. T. Human influences on rates of phenotypic change in wild animal populations. *Mol. Ecol.* **17**, 20–29 (2008).

Acknowledgements

We thank MAPS station operators for collecting and sharing their data. D. Kaschube provided critical data access, assisted by R. Guralnick and R. LaFrance. We thank C. Che-Castaldo for helpful discussions regarding the statistical modelling. Illustrations were provided by L. Helton. Funding was provided by National Science Foundation grants EF 1703048 (M.W.T.) and EF 2033263 (M.W.T.).

Author contributions

C.Y. led formal analysis. C.Y. and M.W.T. shared conceptualization and writing of the original draft. R.B.S. and J.F.S. facilitated data access. All authors contributed to review and editing of drafts.

Competing interests

The authors declare no competing interests.

Additional information

Extended data is available for this paper at https://doi.org/10.1038/s41559-022-01893-x.

Supplementary information The online version contains supplementary material available at https://doi.org/10.1038/s41559-022-01893-x.

Correspondence and requests for materials should be addressed to Casey Youngflesh.

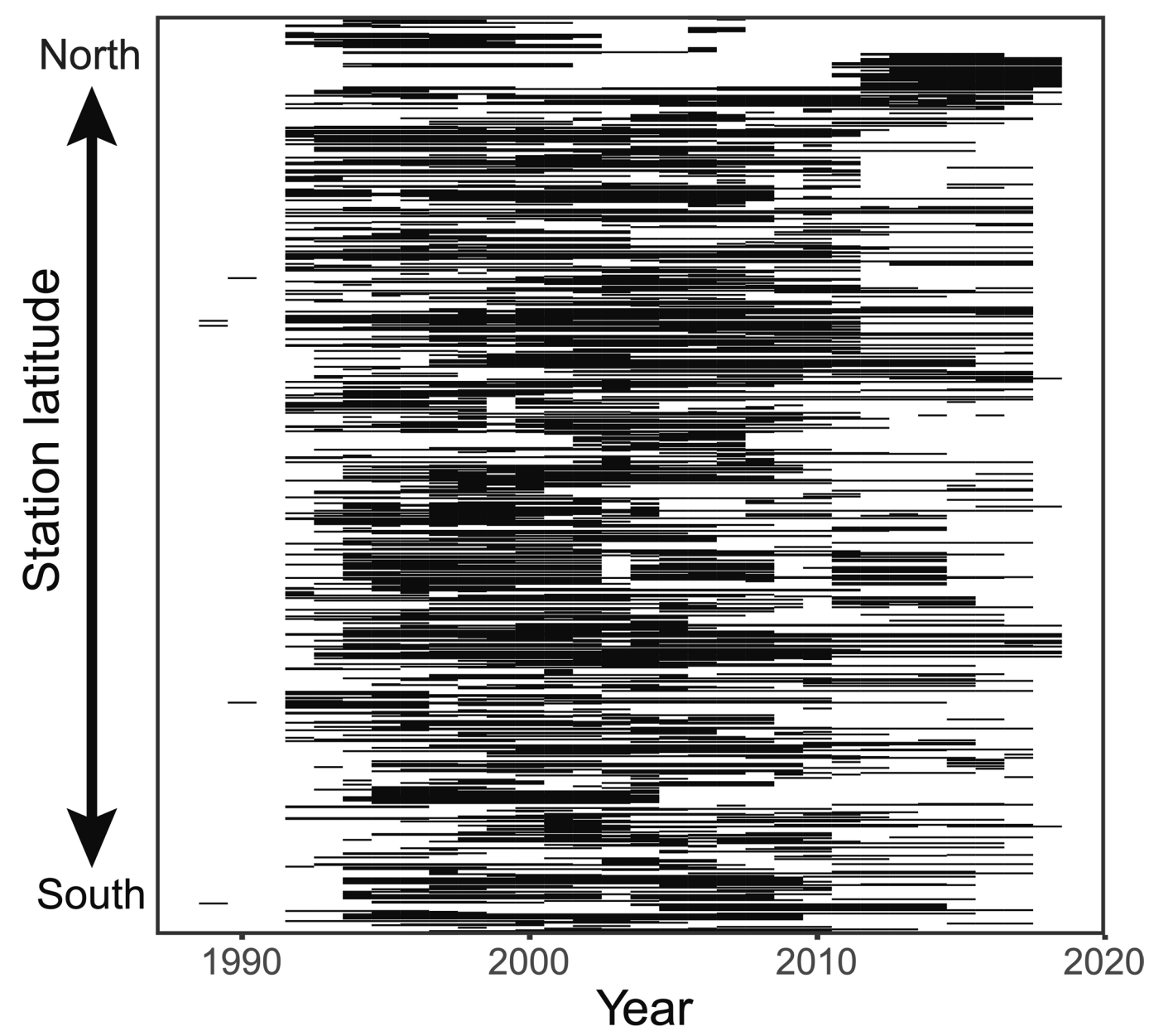
Peer review information *Nature Ecology & Evolution* thanks Nir Sapir and the other, anonymous, reviewer(s) for their contribution to the peer review of this work.

Reprints and permissions information is available at www.nature.com/reprints.

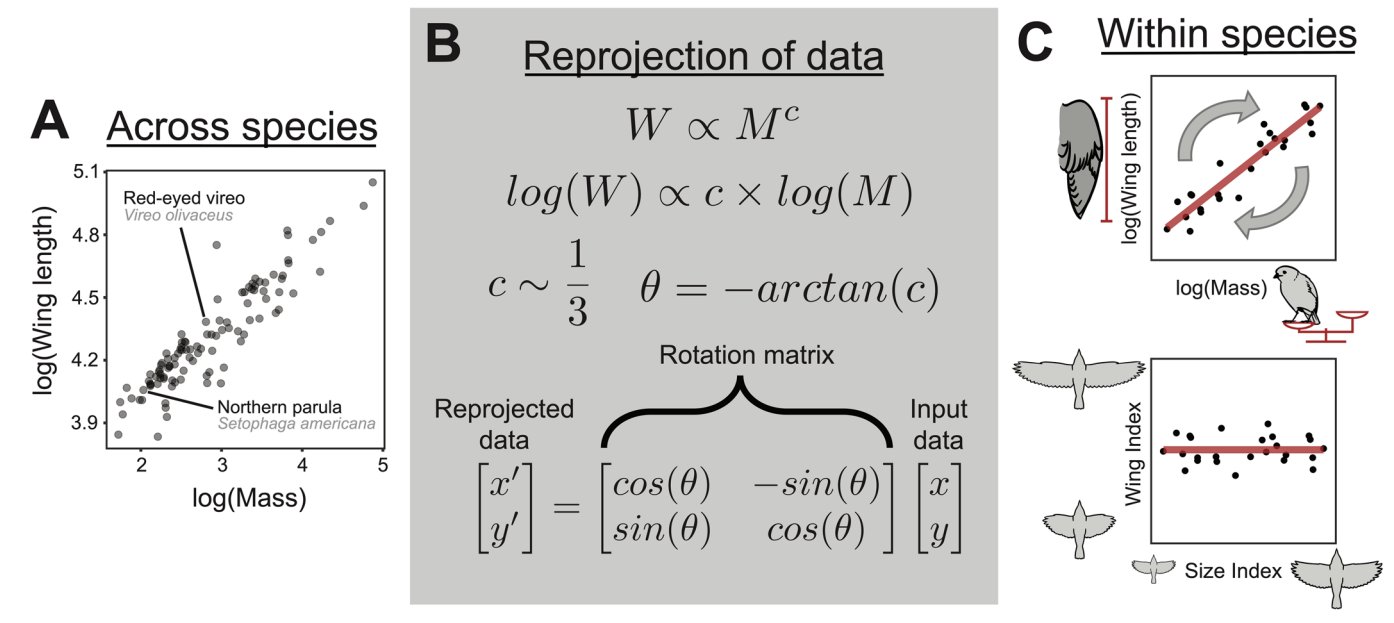
Publisher's note Springer Nature remains neutral with regard to jurisdictional claims in published maps and institutional affiliations.

Springer Nature or its licensor holds exclusive rights to this article under a publishing agreement with the author(s) or other rightsholder(s); author self-archiving of the accepted manuscript version of this article is solely governed by the terms of such publishing agreement and applicable law.

© The Author(s), under exclusive licence to Springer Nature Limited 2022

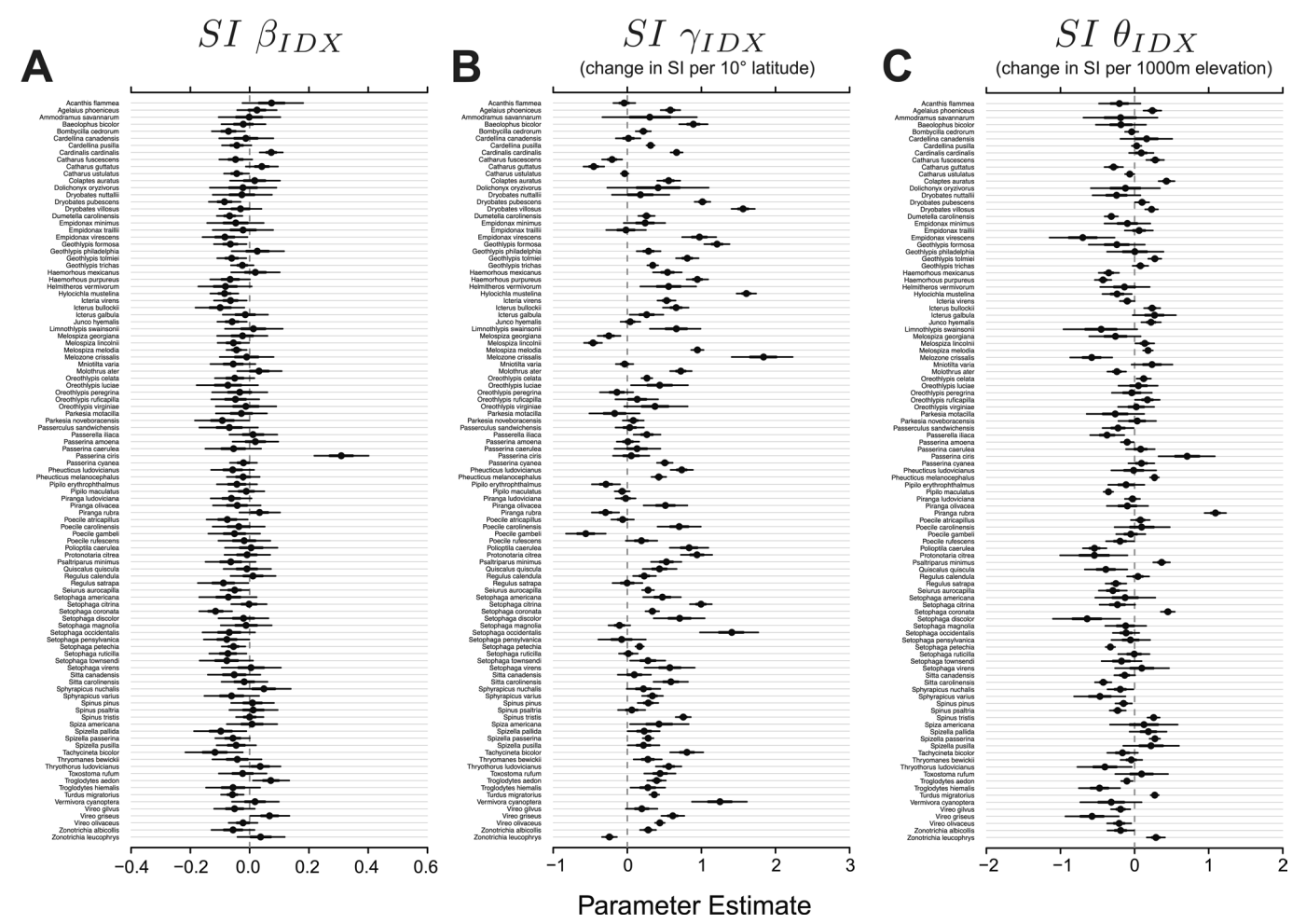


Extended Data Fig. 1 | **Morphological data availability over time.** Each horizontal line represents one of 1124 MAPS stations. Stations are ordered by latitude, from north (top) to south (bottom).



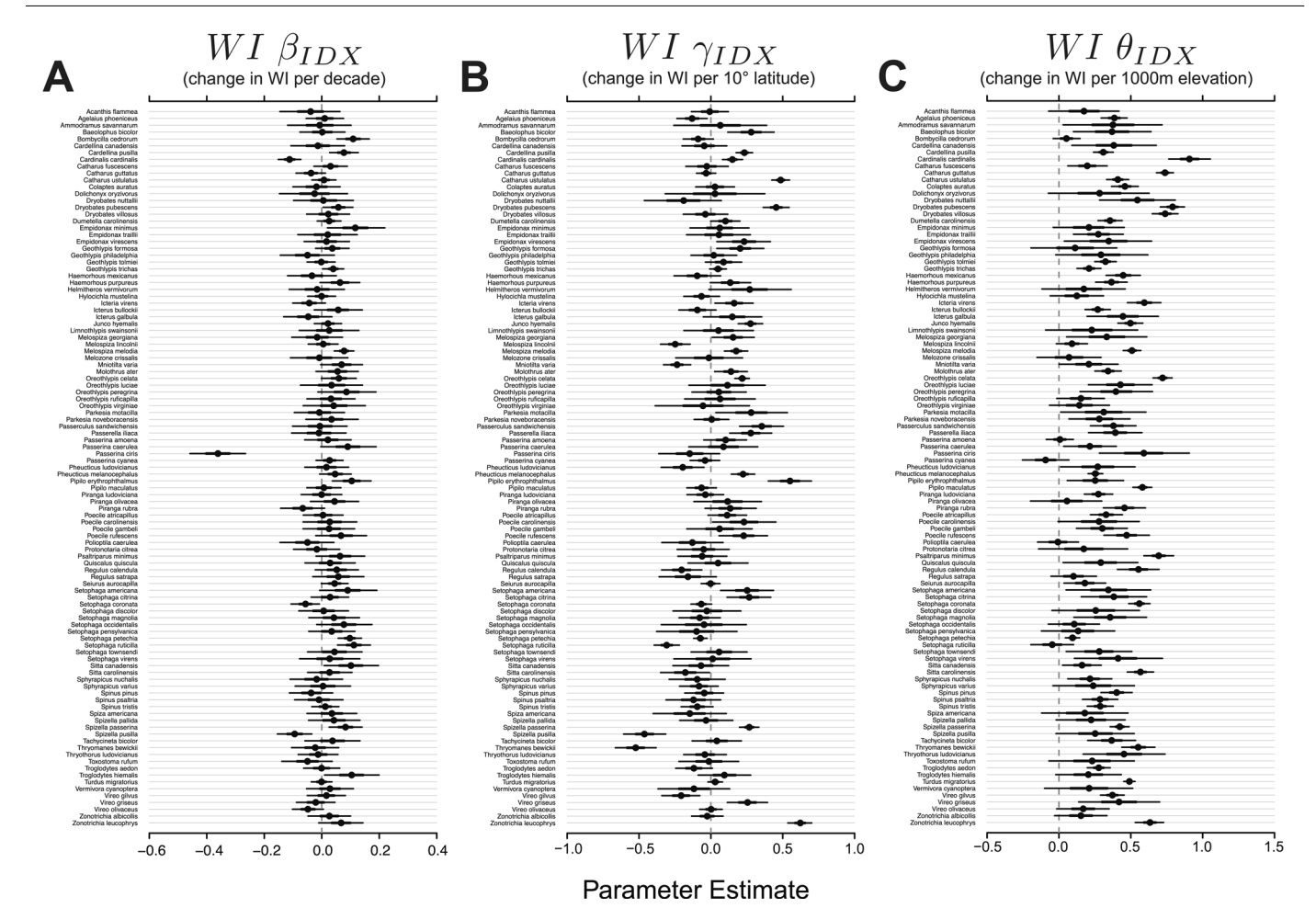
Extended Data Fig. 2 | **Derivation of morphological indices.** (**A**) Logged wing length as a function of logged mass for the 105 bird species considered in this study. Points represent mean values for each species. (**B**) The relationship between wing length (W) and mass (M) can be described by a power law, where c represents the scaling exponent. Logging both sides of the equation linearizes this model. Using a phylogenetic regression, c was estimated to be approximately 1/3 across species, as predicted by scaling theory. The negative arc tangent of this

estimate (to convert the slope to radians) was used to create a rotation matrix. (C) For each species, the rotation matrix was used to reproject logged wing length and logged mass onto a new coordinate plane (top panel). Values for both the x and y axes were standardized to have a standard deviation of 1, to create a size index and wing index, representing the overall size of each individual bird and the degree to which wing length deviates from its expected value given the body mass of the individual, respectively (bottom panel).



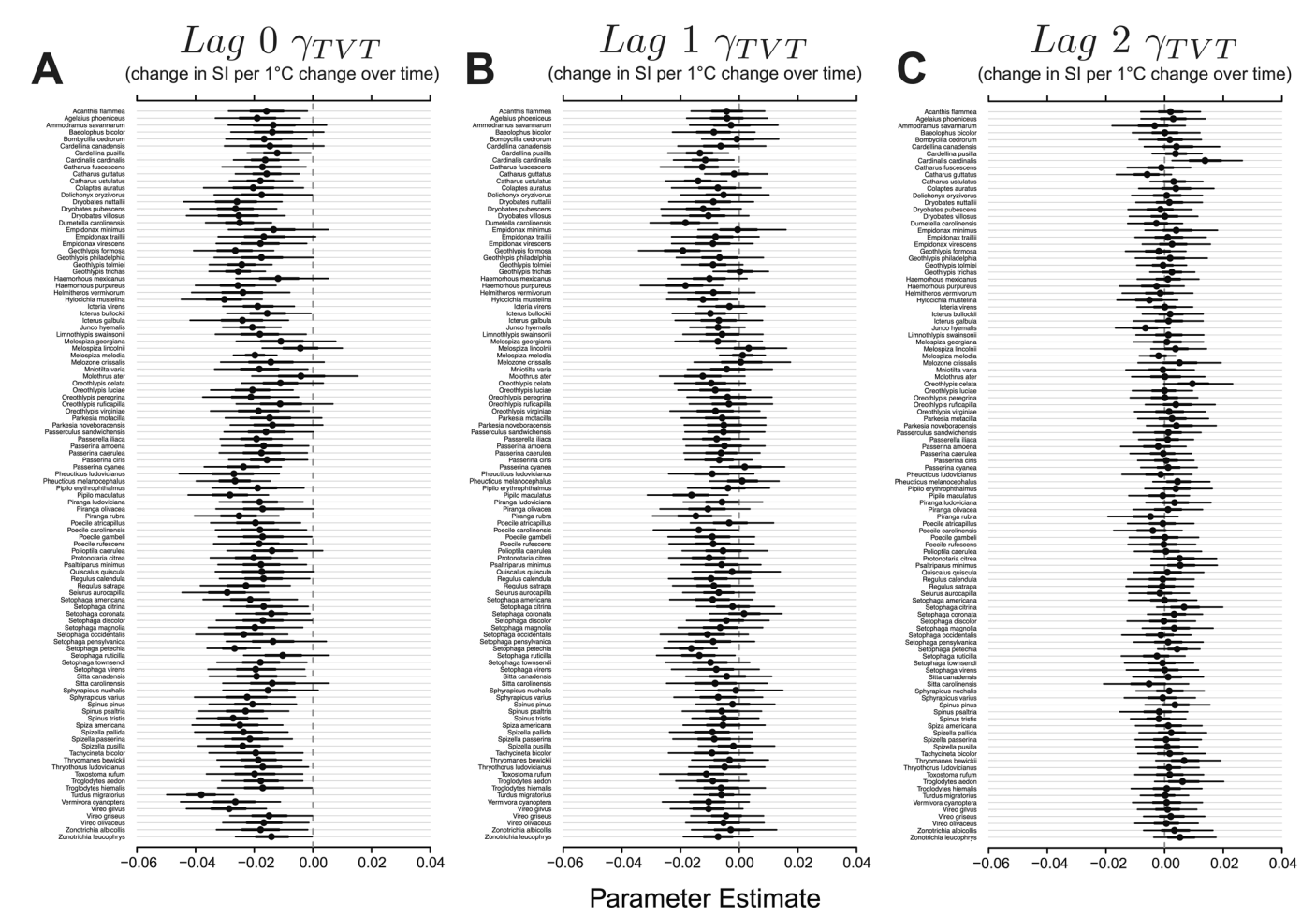
Extended Data Fig. 3 | Posterior estimates for (A) $SI\beta_{\rm IDX}$ (Eq. 6), (B) $SI\gamma_{\rm IDX}$ (Eq. 11), and (C) $SI\theta_{\rm IDX}$ (Eq. 11), denoting the change in size index for each species per 10 years, 10 degrees latitude, and 1000 m elevation, respectively.

Points represent the posterior medians, while thick and thin lines represent the 50% and 89% credible intervals, respectively. The dashed grey line represents zero in all cases.



Extended Data Fig. 4 | Posterior estimates for (A) $WI\beta_{\rm IDX}$ (Eq. 6), (B) $WI\gamma_{\rm IDX}$ (Eq. 11), and (C) $WI\theta_{\rm IDX}$ (Eq. 11), denoting the change in wing index for each species per 10 years, 10 degrees latitude, and 1000 m elevation, respectively.

Points represent the posterior medians, while thick and thin lines represent the 50% and 89% credible intervals, respectively. The dashed grey line represents zero in all cases.

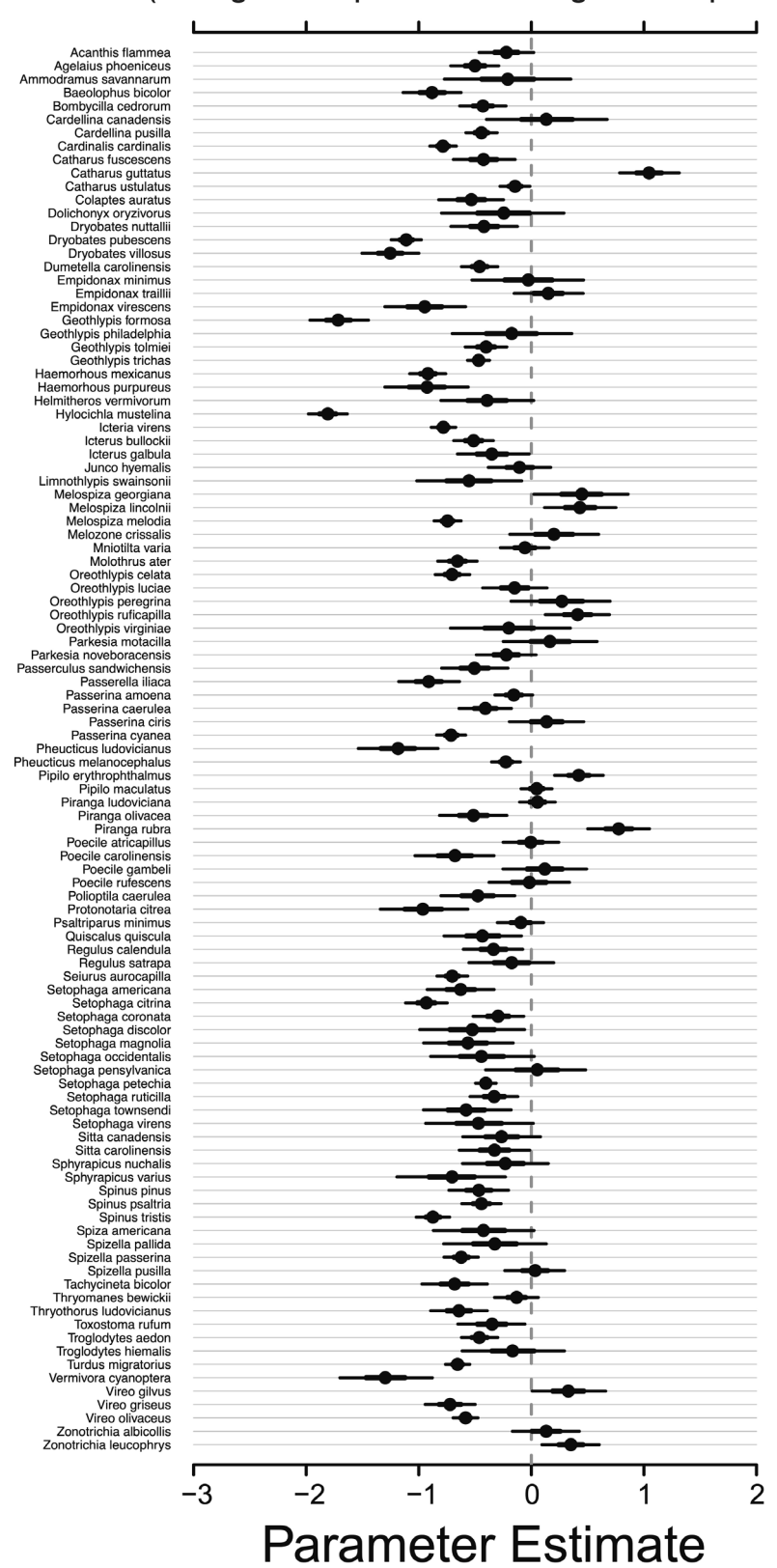


Extended Data Fig. 5 | Posterior estimates for (A) Lag 0 γ_{TVT} (Eq. 15), (B) Lag 1 γ_{TVT} (Eq. 15), and (C) Lag 2 γ_{TVT} (Eq. 15), denoting the change in Size Index for each species per 1C change in temperature at lag 0, lag 1, lag 2, respectively

(i.e., the effect of change in temperature over time). Points represent the posterior medians, while thick and thin lines represent the 50% and 89% credible intervals, respectively. The dashed grey line represents zero in all cases.

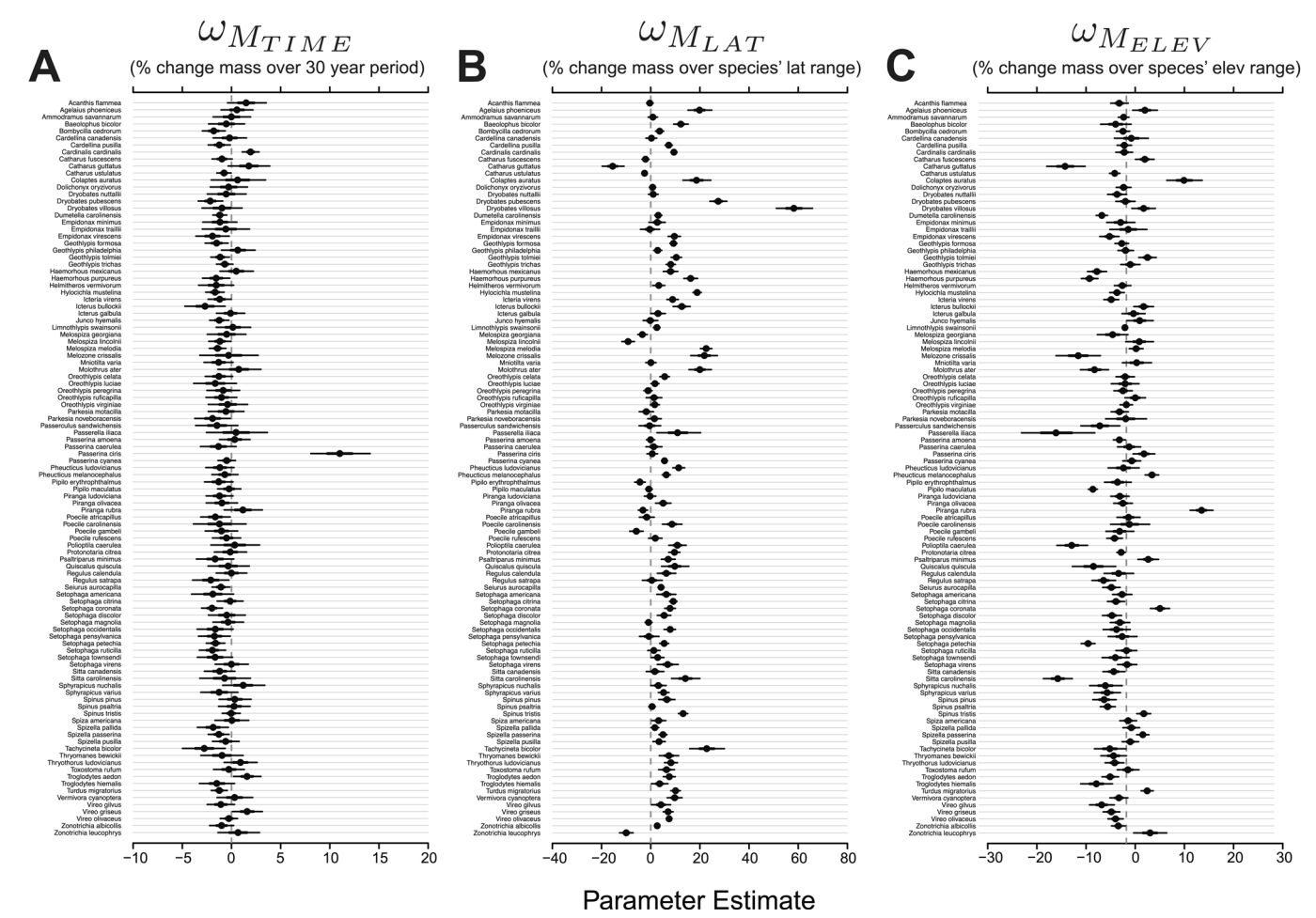


(change in SI per 10°C change over space)



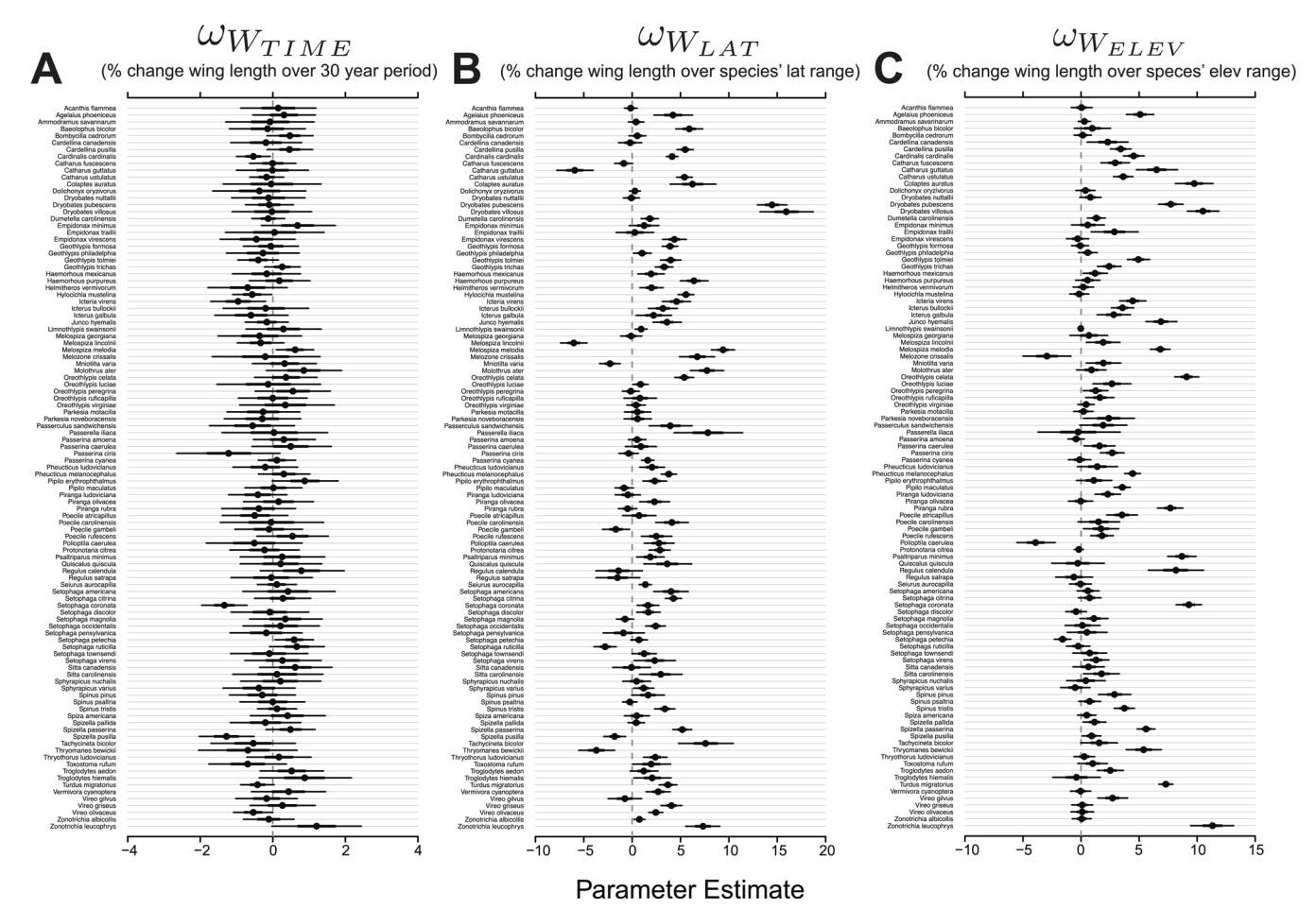
Extended Data Fig. 6 | Posterior estimates for β_{SVT} (Eq. 19) denoting the change in size index for each species per 10 °C change in mean station temperature (i.e., the effect of change in temperature over space). Points

represent the posterior medians, while thick and thin lines represent the 50% and 89% credible intervals, respectively. The dashed grey line represents zero in all cases.



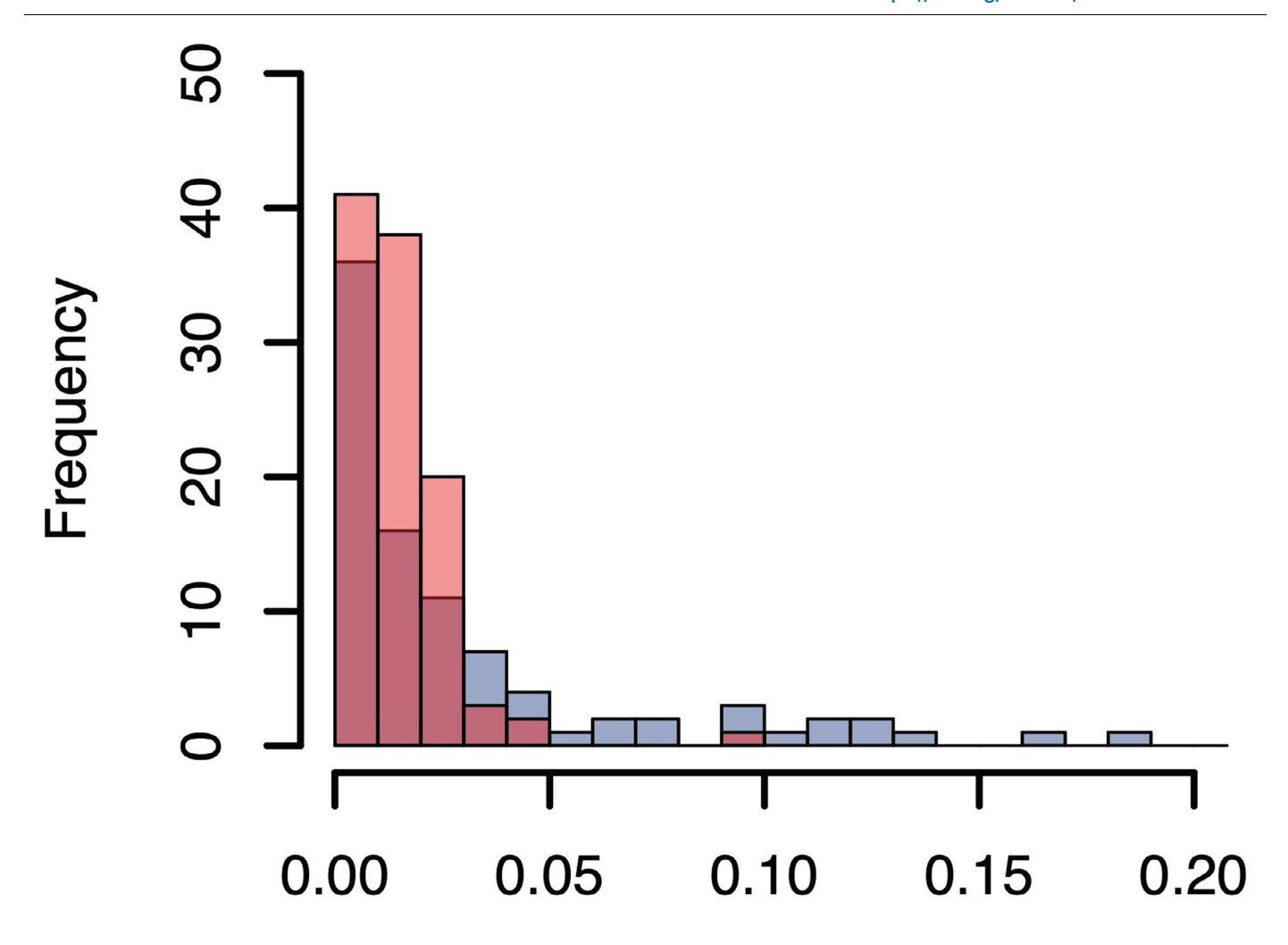
Extended Data Fig. 7 | Posterior estimates for (A) $\omega_{M_{\text{TIME}}}$ (Eq. 25), (B) $\omega_{M_{\text{LAT}}}$ (Eq. 25), and (C) $\omega_{M_{\text{ELEV}}}$ (Eq. 25), denoting the percent change in mass for each species over the 30-year study period, the latitudinal range across which each species was sampled, and the elevational range across which each

species was sampled, respectively. Points represent the posterior medians, while thick and thin lines represent the 50% and 89% credible intervals, respectively. The dashed grey line represents zero in all cases.



Extended Data Fig. 8 | Posterior estimates for (A) $\omega_{W_{\text{TIME}}}$ (Eq. 25), (B) $\omega_{W_{\text{LAT}}}$ (Eq. 25), and (C) $\omega_{W_{\text{ELEV}}}$ (Eq. 25), denoting the percent change in wing length for each species over the 30-year study period, the latitudinal range across which each species was sampled, and the elevational range across which each

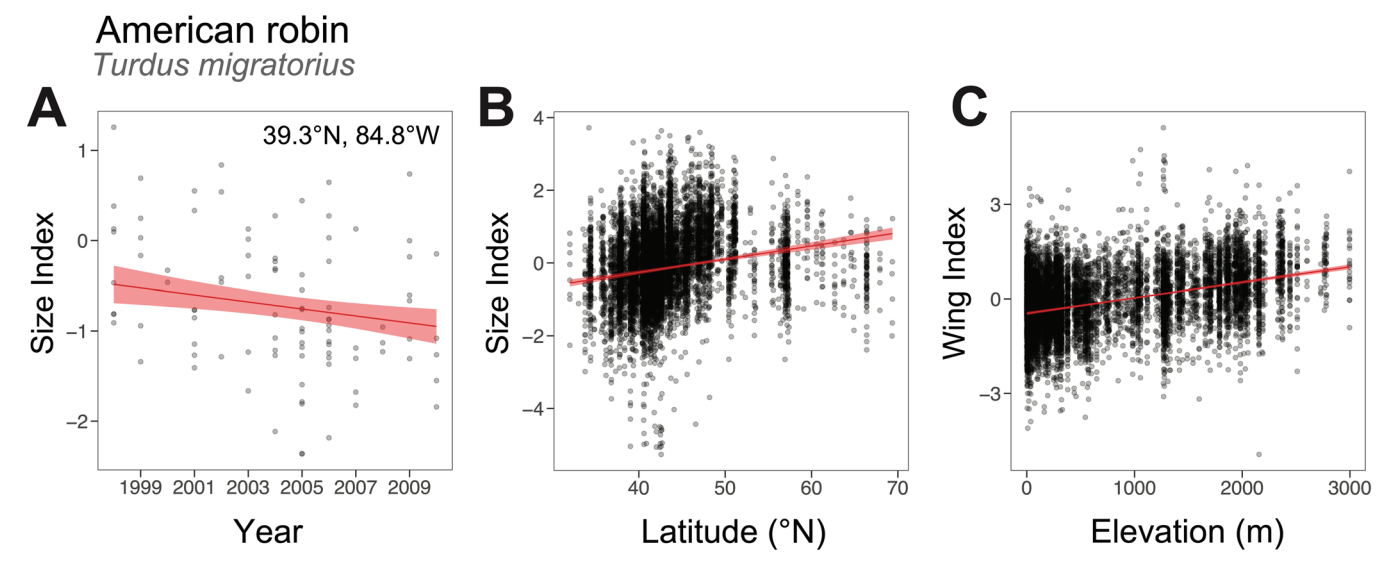
species was sampled, respectively. Points represent the posterior medians, while thick and thin lines represent the 50% and 89% credible intervals, respectively. The dashed grey line represents zero in all cases.



Rate of phenotypic change (haldanes)

Extended Data Fig. 9 | Absolute value of the estimate rate of change (represented in units of haldanes [standard deviations per generation]) for body mass (|h|) for focal species in this study (red) and for species and

traits presented in (79) (blue). Traits considered by (79) varied by species and only species undergoing anthropogenic disturbance [as defined by (79)] were considered. The x-axis of the plot is truncated at 0.2 to facilitate visualization.



Extended Data Fig. 10 | General trends (decrease in SI over time, increase in SI over latitude, and increase in WI over elevation) observed in this study as exhibited by $Turdus\ migratorius\ (American\ robin)$. (a) Observed size index measures at one MAPS banding station (located at 39.3°N, 84.8°W) plotted over

time. **(b)** Observed size index measures plotted across latitude. **(c)** Observed wing index measures plotted across elevation. In all cases, each black point represents one individual, the posterior mean of the linear predictor is plotted in red, while the red ribbon represents the 89% CI.

nature portfolio

Corresponding author(s):	Casey Youngflesh
Last updated by author(s):	Aug 9, 2022

Reporting Summary

Nature Portfolio wishes to improve the reproducibility of the work that we publish. This form provides structure for consistency and transparency in reporting. For further information on Nature Portfolio policies, see our Editorial Policies and the Editorial Policy Checklist.

For all statistical analyses, confirm that the following items are present in the figure legend, table legend, main text, or Methods section.

_				
ς.	ŀа	t١	ict	icc

n/a	Confirmed
	\square The exact sample size (n) for each experimental group/condition, given as a discrete number and unit of measurement
	A statement on whether measurements were taken from distinct samples or whether the same sample was measured repeatedly
	The statistical test(s) used AND whether they are one- or two-sided Only common tests should be described solely by name; describe more complex techniques in the Methods section.
	A description of all covariates tested
	A description of any assumptions or corrections, such as tests of normality and adjustment for multiple comparisons
	A full description of the statistical parameters including central tendency (e.g. means) or other basic estimates (e.g. regression coefficient) AND variation (e.g. standard deviation) or associated estimates of uncertainty (e.g. confidence intervals)
\boxtimes	For null hypothesis testing, the test statistic (e.g. <i>F</i> , <i>t</i> , <i>r</i>) with confidence intervals, effect sizes, degrees of freedom and <i>P</i> value noted <i>Give P values as exact values whenever suitable.</i>
	For Bayesian analysis, information on the choice of priors and Markov chain Monte Carlo settings
	For hierarchical and complex designs, identification of the appropriate level for tests and full reporting of outcomes
	Estimates of effect sizes (e.g. Cohen's <i>d</i> , Pearson's <i>r</i>), indicating how they were calculated
	Our web collection on <u>statistics for biologists</u> contains articles on many of the points above.
So	ftware and code
Poli	cy information about <u>availability of computer code</u>

Data collection

No software used for data collection

Data analysis

All analyses were conducted using R 4.1.1. R packages used include: tidyverse 1.3.1 (R package), ape 5.5 (R package), caper 1.0.1 (R package), gdalUtils 2.0.3.2 (R package), sp 1.4-6 (R package), rstan 2.21.3 (R package), MCMCvis 0.15.5 (R package), phytools 1.0-1 (R package), viridis 0.6.2 (R package), raster 3.5-2 (R package), tmap 3.3-2, sf 1.0-4 (R package)

All code used for analyses is available on Github (https://github.com/caseyyoungflesh/MAPS_morph_changes) and is archived on Zenodo (https://doi.org/10.5281/zenodo.6975694).

For manuscripts utilizing custom algorithms or software that are central to the research but not yet described in published literature, software must be made available to editors and reviewers. We strongly encourage code deposition in a community repository (e.g. GitHub). See the Nature Portfolio guidelines for submitting code & software for further information.

Data

Policy information about availability of data

All manuscripts must include a data availability statement. This statement should provide the following information, where applicable:

- Accession codes, unique identifiers, or web links for publicly available datasets
- A description of any restrictions on data availability
- For clinical datasets or third party data, please ensure that the statement adheres to our policy

Data from the Monitoring Avian Productivity and Survivorship (MAPS) program are curated and managed by The Institute for Bird Populations and were queried from the MAPS database on 2019-10-16. MAPS data is archived on Dryad (https://doi.org/10.5068/D1DT2T).

— ·			c·			
\vdash I \cap	IM-c	peci ⁻	tic .	$r \rho n$	\cap rtı	na
	iu s	PCCI		$\Gamma \subset \mathcal{P}$	OI LI	אוו

rieia-specifi	z reporting		
Please select the one below	v that is the best fit for your research. If you are not sure, read the appropriate sections before making your selection.		
Life sciences	☐ Behavioural & social sciences ☐ Ecological, evolutionary & environmental sciences		
For a reference copy of the docum	ent with all sections, see <u>nature.com/documents/nr-reporting-summary-flat.pdf</u>		
Ecological, e	volutionary & environmental sciences study design		
All studies must disclose or	these points even when the disclosure is negative.		
Study description	We evaluated how the intraspecific morphology of 105 bird species varies across the North American continent and over a period of 30 years (1989-2018), and how the overall size of birds varies in response to fluctuations in temperature.		
Research sample	We used morphological data from 253,488 captures of 105 bird species, representing two orders and 18 taxonomic families at locations spanning approximately 43 degrees of latitude and 2996 meters of elevation. These data were derived from the Monitoring Avian Productivity and Survivorship (MAPS) program, a large-scale bird banding program. Only species with at least 375 MAPS capture records were used for analyses in order to make statistical inference on intraspecific morphological variation, as described in the Methods section. Species included in the study, sample sizes, and latitudinal and elevation sampling ranges as presented in the supplementary materials.		
Sampling strategy	Data collection was performed as a part of the MAPS program. See 'Research sample' for more information on the data used.		
Data collection	All data were collected according the MAPS program protocols, as part of the MAPS program.		
Timing and spatial scale	We used all MAPS data from 1989-2018 from all MAPS banding stations. The temporal sampling for each station is presented in the supplementary materials, as are the samples sizes and spatial sampling ranges for each species.		
Data exclusions	For each species, morphological records more than five median absolute deviations away from the median (considered extreme outliers) were excluded, as these records likely represented measurement or data entry errors.		
Reproducibility	No experiments were conducted. All code is available on Gihub and will be archived on Zenodo upon acceptance. All data will be archived on Dryad upon acceptance.		
Randomization	No experiments or randomizations were conducted.		
Blinding	No treatment group was used, so no blinding was necessary.		
Did the study involve field	d work? Yes No		
Reporting fo	r specific materials, systems and methods		
We require information from a	nuthors about some types of materials, experimental systems and methods used in many studies. Here, indicate whether each material, evant to your study. If you are not sure if a list item applies to your research, read the appropriate section before selecting a response.		
Materials & experime	ntal systems Methods		
n/a Involved in the study	n/a Involved in the study		
Antibodies	ChIP-seq		
Eukaryotic cell lines	Flow cytometry		
Palaeontology and a			
Animals and other o			
Human research pa Clinical data	rucipants		
Dual use research o	froncern		
Z Dual use research o			
Animals and othe	r organisms		
Policy information about st	udies involving animals; ARRIVE guidelines recommended for reporting animal research		
Laboratory animals	No laboratory animals were used in this study.		
Wild animals	Birds were captured in accordance with protocols set forth by the United States Geological Survey Bird Banding Laboratory and data		

collected in accordance with MAPS protocols.

Field-collected samples No field-collected samples were used.

Ethics oversight

All birds were captured and banded by MAPS participants under bird banding permits issued by the United States Geological Survey Bird Banding Laboratory.

Note that full information on the approval of the study protocol must also be provided in the manuscript.